ELEMENTA
Science of the Anthropocene

Gerosa, GA, et al. 2022. Interannual variability of ozone fluxes in a broadleaf deciduous forest in Italy. *Elem Sci Anth*, 10: 1.
DOI: https://doi.org/10.1525/elementa.2021.00105

RESEARCH ARTICLE

Interannual variability of ozone fluxes in a broadleaf deciduous forest in Italy

Giacomo A. Gerosa[1], Riccardo Marzuoli[1,*], and Angelo Finco[1]

Multiannual measurements of ozone (O_3) fluxes were performed from 2012 to 2020 in a broadleaf deciduous forest of the Po Valley, Italy. Fluxes were measured with the eddy covariance technique on a 41-m high tower, 15 m above the forest canopy. Different partition methodologies, based on concomitant water and carbon dioxide measurements, were compared for the calculation of the stomatal and non-stomatal components of the O_3 fluxes. Total O_3 fluxes revealed a marked interannual variability that was mainly driven by the stomatal activity in summer. Therefore, those factors that influence stomatal conductance were responsible for the flux variability, with soil water content being the main physiological driver. Despite the variability of the total O_3 fluxes, the annual mean of the stomatal fraction was similar in the different years, around 42% on a 24-h basis, with an average summer value of 52% and a maximum around 60% during the summer daylight hours. The non-stomatal deposition was mainly driven by air humidity, surface wetness, and chemical sinks such as reaction of O_3 with nitric oxide. Wind speed, turbulence intensity, and surface temperature showed a negative relationship with the non-stomatal fraction, but this was probably the result of a temporal misalignment between the daily cycles of non-stomatal conductance and those of temperature, turbulence, and wind speed. During the 7 years of measurements, the forest experienced a phytotoxic O_3 dose of 10.55 mmolO_3 m^{-2}, as annual average, with an estimated reduction of the forest growth rate around 3% yr^{-1} according to the dose–effect relationships of the United Nations Economic Commission for Europe for broadleaf deciduous forests. Besides their implication for the O_3 risk assessment for vegetation, these long-term measurements could be useful to test the deposition models used to correctly assess the O_3 budget in troposphere on a multiannual time span.

Keywords: Ozone fluxes, Stomatal and non-stomatal fluxes, Multiannual measurements, Surface conductance, Eddy covariance, Broadleaf deciduous forest

Introduction

Ozone (O_3) deposition on vegetation has been a topic of interest for the scientific community for 4 decades now (e.g., Wesely et al., 1978; Neumann and Den Hartog, 1985; Fan et al., 1990), as regards both the quantification of the O_3 budget in the troposphere and the evaluation of the impacts on vegetation. In fact, O_3 is a well-known threat to vegetation, being responsible for a series of negative effects ranging from the onset of visible leaf symptoms to significant reductions of plants photosynthetic performance and growth rate (Ashmore, 2005; Wittig et al., 2009; Marzuoli et al., 2019; Emberson, 2020).

Many efforts have been made in the past to measure the O_3 deposition on different terrestrial ecosystems, both in agricultural (e.g., Grantz et al., 1997; Gerosa et al., 2003; Lamaud et al., 2009) and forest sites (e.g., Rannik et al., 2012; Fares et al., 2014; Finco et al., 2017), and in particular to correctly quantify the stomatal dose absorbed by vegetation. Indeed, the negative effect of O_3 on plants is more related to the amount of pollutant taken up by leaves through stomata than the simple cumulative exposure. Ozone, in fact, can enter the leaf only through stomata, because deposition on the leaf cuticle and other plant surfaces tends to cause the disruption of the molecule (Cape et al., 2009). For this reason, the O_3 critical levels for the protection of vegetation have been recently redefined by the United Nations Economic Commission for Europe (UNECE) with the introduction of the Phytotoxic Ozone Dose (POD*y*), that is, the cumulative stomatal flux of O_3 above a detoxification threshold *y* (Convention on Long-Range Transboundary Air Pollution [CLRTAP], 2017). The O_3 dose absorbed by vegetation strongly depends on the environmental factors that influence the physiological regulation of stomata (Emberson et al., 2000), particularly on the soil water availability, which is directly correlated to the O_3 stomatal flux (Lin et al., 2020).

On the other hand, many studies have highlighted that the non-stomatal processes can play an important

[1] Department of Mathematics and Physics, Catholic University of the Sacred Heart, Brescia, Italy

* Corresponding author:
Email: riccardo.marzuoli@unicatt.it

(Fowler et al., 2009) or even dominant (Gerosa et al., 2005; Gerosa et al., 2009a; Clifton et al., 2017) role in the total O_3 deposition on an ecosystem (i.e., the total amount of O_3 removed from the troposphere). These processes include the physical deposition processes and air chemistry reactions that lead to O_3 consumption, such as the deposition on dry and wet surfaces (Altimir et al., 2006; Cape et al., 2009), the deposition on soil (Stella et al., 2011) and chemical reactions with nitric oxide (NO) (Rummel et al., 2007) and biogenic volatile organic compounds (BVOCs) (Goldstein et al., 2004). A comprehensive review of the O_3 stomatal and non-stomatal deposition processes in forests, crops, water, and cryosphere can be found in Clifton et al. (2020), who also proposed a mechanistic formulation for the 2 main non-stomatal deposition pathways: deposition on dry and wet cuticles and deposition on soil. Those formulations, however, still need to be tested with new long-term measurements.

In fact, current knowledge of O_3 dry deposition is mainly based on a few O_3 flux datasets, often covering only short-time periods (Clifton et al., 2020; He et al., 2021). Only few multiannual series of O_3 flux measurements are available for forests (Mikkelsen et al., 2004; Neirynck et al., 2012; Rannik et al., 2012; Neirynck and Verstraeten, 2018), even though multiannual measurements are currently running at the Amazon Tall Tower Observatory (Andreae et al., 2015) and at the Virginia Forest Research Facility in the United States. In the temperate zone, some long-term O_3 flux measurements are available for evergreen, coniferous, and mixed forests (e.g., Lamaud et al., 2002; Gerosa et al., 2005; Hogg et al., 2007; Neirynck et al., 2012; Fares et al., 2014), but similar measurements for deciduous forest are still missing, except for a few short campaigns (Fuentes et al., 1992; Munger et al., 1996; Finkelstein et al., 2000; Michou et al., 2005; Le Morvan-Quéméner et al., 2018). A complete annual series of O_3 fluxes was reported by Zona et al. (2014) for a poplar plantation in Belgium. However, to our knowledge, the only multiannual O_3 flux series available for a deciduous forest so far is that reported by Clifton et al. (2017) for the Harvard Forest in Northeastern United States, although this ecosystem is not a pure deciduous forest, because it includes a minor percentage of conifers. Clifton et al. (2017) highlighted that for this site the interannual variability of O_3 fluxes could not be explained by meteorology and was largely attributable to non-stomatal deposition, as also concluded by Rannik et al. (2012) in their analysis of a long-term O_3 flux series taken in an evergreen coniferous forest in Hyytiälä (Finland).

Multiannual measurements of O_3 fluxes are therefore needed on the one hand to investigate the reason for the interannual variability, and on the other hand, to get solid data against which to evaluate the factors that influence both stomatal and non-stomatal deposition. Thus, our multiannual O_3 flux measurements in a pure deciduous temperate forest (i.e., without any conifer in their composition) aim to help close some of the knowledge gaps highlighted by Clifton et al. (2020) such as assessing the temporal variability of deposition processes and the contribution of stomatal uptake and chemistry of the canopy air to O_3 dry deposition. The studied forest is located in the Po Valley (northern Italy), within an aerological basin of great interest because of the high levels of air pollution and photooxidants in the summer season (Gerosa and Ballarin-Denti, 2003). In this forest, ecosystem-level O_3 flux measurements have been underway since 2012 as a follow-up to the European project ÉCLAIRE (2011–2015) aimed at evaluating the Effects of Climate Change on Air Pollution and Response Strategies for European Ecosystems (https://cordis.europa.eu/project/id/282910/reporting).

The objectives of this study are (1) to investigate the interannual, seasonal, and day-to-day variability of the O_3 fluxes in this forest type, (2) to assess the relative importance of stomatal and non-stomatal deposition, (3) to compare different partitioning approaches (based on H_2O and CO_2 fluxes) for the correct estimation of the canopy stomatal uptake, (4) to investigate the effect of the O_3 storage on the diurnal course of the O_3 deposition, (5) to identify the main environmental drivers of the temporal variability of the summertime fluxes, and (6) to assess the phytotoxic O_3 dose absorbed by the plants during the growing season and the related potential damage to plants. An additional purpose is to share a new multiannual database of O_3 fluxes that could help to improve and calibrate O_3 deposition models, to test models' ability to reproduce interannual variations, and to verify the performances of different O_3 risk estimation metrics for forests on a multiannual basis.

Methodology

Site description

The study site is a 235 hectare mature Oak-Hornbeam forest at the outskirts of the city of Mantua, in the middle of the Po Valley, Italy. It is a natural reserve named "Bosco della Fontana" declared by the European Union as Site of Community importance and Special Protection Zone of the network Natura 2000 (site code IT20B0011). The forest is one of the last remnants of the flood plain forests that covered the Po Valley in the past.

The dominant tree species are *Carpinus betulus* and *Quercus robur*, but *Acer campestre*, *Prunus avium*, *Fraxinus ornus* and *oxycarpa*, *Ulmus minor*, and *Alnus glutinosa* are also present. The canopy is closed and the mean canopy height is 26 m. The understorey is formed by *Corylus avellana*, *Sambucus* spp, *Cornus mas*, *Crataegus oxyacantha* and *monogyna* and *Sorbus torminalis*, with a shrubs layer of evergreen and semideciduous species (*Ruscus aculeatus*, *Hedera helix*, *Rubus ulmifolius*). A few individuals of alien species are also present in the forest: *Quercus rubra, Juglans nigra, Platanus orientalis* and *Robinia pseudoacacia.*

The growing season ranges from April to October: leaves emerge around mid-April and last on the trees until November. In the autumn–winter months, only grasses and evergreen understorey vegetation are active. The canopy Leaf Area Index (LAI) was measured periodically in the forest acquiring hemispherical photos with a Sigma 8 mm fisheye lens mounted on a Canon 400D camera. The digital elaboration of the canopy images was made with Hemisfer 3.0 software (WSL Switzerland). The annual

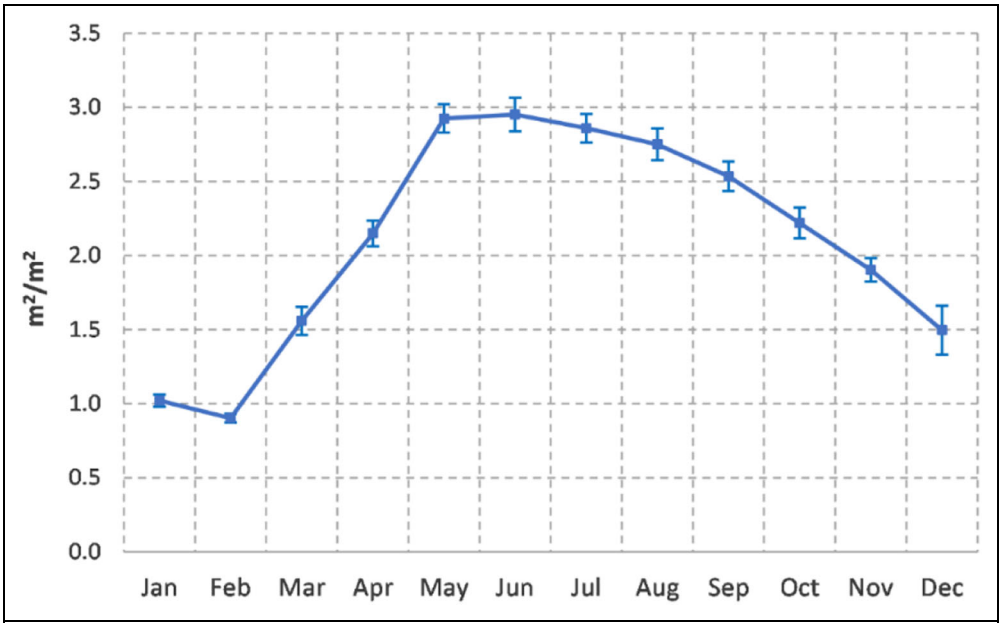

Figure 1. Canopy Leaf Area Index (LAI). Annual evolution of the canopy LAI at Bosco Fontana calculated from hemispherical photos. Vertical bars represent the standard error of the mean.

evolution of LAI (**Figure 1**) shows values between 2.5 and 3.0 m^2 m^{-2} during the summer season, with a steep increment from 0.9 m^2 m^{-2} in the first weeks after leaf emergence and a slow decrease starting from September.

For decades, the forest management has been oriented toward reaching "old growth forest" status (Peterken, 1996), with no significant management except for the eradication of some alien species introduced during the 1950s and the retention of the woody debris to preserve the arthropod and bird biodiversity of the reserve.

The aspect is flat (25 m a.s.l.) and the soil is a loamy skeletal, mixed, mesic Petrocalcic Palexeralf (Campanaro et al., 2007) according to the USDA classification. The soil depth is 1.5 m, but a petrocalcic hardened layer, formed after the gradual deepening of the water table, lies between 0.80 and 1 m depth.

The site climate is typical of the Po Valley, with cold winters and hot summers (Longo, 2004). The mean annual temperature is 13.2°C (period 1840–1997; Bellumè et al., 1998), with an average temperature of 1.3°C in the coldest month (January) and 24.6°C in the warmest month (July). The mean annual precipitation is 658 mm with 2 maxima in May and October, and 2 minima in February and July. A period of hydrological deficit generally occurs in July, due to the combination of temperature and precipitation conditions. However, plants can rely on the underground aquifer as the water table can as shallow as 1.5 m below ground. The prevailing winds are generally from the East (E) and North-East (NE), particularly in spring and summer.

Instruments

Inside the natural reserve, a 41-m scaffolding tower was installed in 2012 (45°11′52.27" N, 10°44′32.27" E) as part of the research infrastructure of the European FP7 Project ÉCLAIRE. The distance of the tower from the forest edge ranges between a minimum of 390 m to the South (S) and a maximum of 1,440 m to the NE.

The walk-up tower is equipped with a sonic anemometer at the top (METEK USA-1, D), along with a LI-7500 (Li-Cor, USA) for CO_2 and H_2O flux measurements, and a chemiluminescence fast O_3 analyzer (COFA, Ecometrics, I), for the O_3 flux measurements. The latter is a clone of the GFAS sensor (Güsten et al., 1992) and required consumable disks of coumarin which have been replaced every 4 days. In order to correct the sensitivity decay of the coumarin disks, a conventional UV photometer (mod. O342 M, Environnement, France) was used as a reference for the chemiluminescence O_3 analyzers (for details, please refer to Finco et al., 2018). The conventional O_3 analyzer was calibrated every 6 months with a primary standard reference analyzer provided by Cosmic Technology s.r.l. (Italy).

In 2018, a second sonic anemometer (METEK USA-1, D), a second COFA and a fast hygrometer KH20 (Campbell sci., USA) were also installed below canopy at 8 m above ground level (a.g.l.) for about 1 year. Moreover, starting from 2018, hourly nitrogen oxides (NO_x) mole fractions were measured 1 m above the soil surface with an APNA 360 analyzer (Horiba, Japan).

At the top of the tower, sensors of incoming and reflected solar photosynthetically active radiation (PAR quantum sensors LI-190, LICOR, USA), air temperature and humidity (E2-ACT, Rotronic, Germany), air pressure (PTB101B, Vaisala, Finland), net radiation (NR-LITE, Kipp&Zonen, Netherlands), precipitation (rain gauge 52202, Young, USA), and leaf wetness (237-L, Campbell sci., USA) were also installed. A second Young tipping gauge was installed on the forest floor to measure precipitation below canopy. Along the vertical profile, temperature, and humidity probes (E2-ACT, Rotronic, Germany) were installed at 20 cm a.g.l., 1 m a.g.l., and then every 8 meters up to the top.

Soil temperature probes (PT100, GMR Strumenti, Italy) were placed in the soil at 5, 30, and 60 cm depth. Three Time Domain Reflectometry sensors (TDR CS616, Campbell sci., USA) were horizontally inserted in the soil to measure the soil volumetric water content, 2 of them at 30 cm depth and 1 at 100 cm depth. Three soil heat flux plates (HFP01-SC, Hukseflux, Netherlands) have been inserted at 5 cm depth to continuously detect soil heat fluxes.

The sonic anemometers and the other fast instruments were sampled at 20 Hz by a dedicated personal computer (PC), and the raw data were stored in 30-min-long files. Slow sensors were sampled every 30 s by two CR1000 dataloggers (Campbell sci., USA), located at the top and the bottom of the tower. Half-hour averages of the acquired data were automatically stored in a PC.

Additionally, 4 automatic static chambers for CO_2 flux measurements (SassFlux, Ecometrics, Italy), with their dedicated control system, were placed on the ground around the tower to measure the soil respiration (for details, please refer to Gerosa et al., 2014).

Measurements reported in this paper range from January 1, 2013, to December 31, 2020. However, 2016 was excluded from the elaboration and discussion, because of a series of instrumentation and power supply problems that affected the monitoring campaign.

Flux calculation

Half-hour raw averages were processed following the eddy covariance technique (EC). First of all, they were despiked according to Vickers and Mahrt (1997), and the gaps were linearly interpolated following a spline procedure. Then, a double rotation was applied to the instantaneous wind vectors, the first rotation to align the reference system of the sonic anemometer to the mean horizontal wind stream direction, and the second rotation to zero the mean vertical wind component (Lee et al., 2004). Samples with tilt rotation that exceeded 5° were discarded.

The rotated data were linearly detrended (Aubinet et al., 2012) and the fluxes were calculated as the covariance between the fast vertical wind speed and the scalar of interest. For water and O_3 fluxes, the lag which maximized the covariance was chosen. Covariances with lag values that differed from the mode by more than 10% were discarded.

Cospectra were calculated to assess the high frequency flux losses of the fast O_3 sensor, and the correction factors were found by an Ogive-analysis (Rummel et al., 2007). The identified corrections ranged between 0 and 1.5% of the raw O_3 fluxes, according to the stability conditions, with a mean value of 1.02%.

The Schotanus correction (Schotanus et al., 1983) was applied to the sensible heat fluxes, and the WPL correction (Webb et al., 1980) was applied to H_2O, CO_2, and O_3 fluxes to account for density fluctuations.

The correction proposed by Boylan et al. (2014) to account for the sensitivity variations of the coumarin dye in fluctuating air humidity was found to be negligible (peak diurnal value of 0.28 nmol m^{-2} s^{-1}, on average) and, as a consequence, was not applied.

The fulfillment of stationarity conditions was checked according to Foken and Wichura (1996) and nonstationary samples were discarded. Moreover, for the O_3 fluxes elaboration, samples for up to 2 h immediately after every change of the coumarin disks were excluded from the analysis.

For the CO_2, H_2O, O_3, and sensible heat fluxes, the storage flux below the measurement height was calculated according to Rummel et al. (2007), and the fluxes were corrected accordingly. More details on this procedure can be found in Finco et al. (2018). Finally, missing data were filled using the Mean Diurnal Variation method as proposed by Aubinet et al. (2012) and Moffat et al. (2007).

Considering all the missing data and all the data exclusions in the different steps above described, the resulting dataset of flux measurements (i.e., not-gapfilled data) amounted to 53.12% of the total 7 years data.

Flux partition: Stomatal and non-stomatal fluxes

The measured O_3 deposition fluxes in dry canopy conditions were partitioned between the stomatal and non-stomatal components following 3 different approaches.

The first approach derived the canopy scale stomatal resistance from the measurement of water fluxes and by inverting the classical Penman–Monteith equation for evapotranspiration. This approach is based on the energy balance and implicitly assumes that in dry canopies all the observed water fluxes are due to stomatal transpiration. Once the stomatal resistance to O_3 R_{StomO3} is derived, the non-stomatal resistance $R_{NonStomO3}$ is obtained by considering a resistive deposition network where R_{StomO3} and $R_{NonStomO3}$ are set in parallel and their summation is equal to the surface resistance R_C which, in turn, is obtained from the total O_3 deposition resistance minus the atmospheric resistance R_a and the sublaminar resistance R_b. Details can be found in Gerosa et al. (2005).

The second approach derived the canopy scale stomatal resistance from the CO_2 fluxes, as described by Lamaud et al. (2009). This approach is based on the observation that regardless if the canopy is dry or wet, there is a relationship between the stomatal conductance to O_3 $g_{StomO3} = 1/R_{StomO3}$ and the CO_2 assimilation flux (A). The latter can be obtained from the direct measurements of the net ecosystem exchange of CO_2 (NEE) by subtracting the heterotrophic soil respiration flux of CO_2 (R_H). Since the photosynthetic assimilation occurs only with the daylight, g_{StomO3} can be estimated only for diurnal hours.

The third approach was a modification of the first one, where the assumption that all the H_2O fluxes are due to stomatal transpiration was modified. The amount of water transpired by the canopy was estimated by subtracting the H_2O evaporated directly from the soil below the canopy. The latter was taken from the measurements of H_2O fluxes made with EC below canopy in 2018. Then the canopy transpiration obtained was used in the inverted Penman–Monteith equation instead of the latent heat flux (LE), to yield the R_{Stom}. The resistive network, the geometries ($h_{canopy} = 26.0$ m, $z_m = 41.0$ m, $z_0 = 2.6$ m, $d = 17.4$ m), as well as the calculation of R_a and R_b were the same for all the 3 approaches. The big-leaf equivalent

to the forest canopy was assumed as a hypostomatous leaf (Monteith and Unsworth, 2014). Air density (ρ), air specific heat (c_p), and the latent heat of vaporization (λ) were adjusted to the half-hourly conditions of pressure (P), temperature (T), and specific humidity (q). In addition, the diffusion coefficients in air of O_3, CO_2, and H_2O were not considered constant but corrected to the actual T and P conditions following Massman (1998), as for the Schmidt numbers of O_3, CO_2, and H_2O.

Based on the results obtained from the comparison of the 3 abovementioned approaches (see Results), all the presented stomatal and non-stomatal fluxes have been calculated with the third approach.

Calculation of the phytotoxical ozone dose and estimation of the effects

The calculation of the POD*y* index for each year of the experiment was possible thanks to the availability of the O_3 stomatal flux measured. The instantaneous O_3 stomatal fluxes were integrated for the time interval April 1 to September 30 (the growing season for deciduous plants), with the application of an O_3 detoxifying threshold of 1 nmol m^{-2} s^{-1} to account for the detoxification capacity of forest trees (Buüker et al., 2015; CLRTAP, 2017). The estimation of the effects in terms of biomass growth reduction was based on the available dose–response relationships described in the UNECE Mapping Manual (CLRTAP, 2017) which defines the critical levels for the protection of various forest plants species in different geographical contexts. In particular the potential growth reductions due to the POD1 values measured at Bosco Fontana were assessed using the dose–response relationships for the Mediterranean and for the continental broadleaf deciduous forests.

Statistical analysis

The interannual variability of total O_3 fluxes (F_{TotO3}) in response to stomatal (g_{StomO3}) and non-stomatal ($g_{NonStomO3}$) conductance, and to O_3 mole fraction, was evaluated with a 1-way analysis of variance (ANOVA) on the highest monthly mean of F_{TotO3} recorded in each year always in July. Stomatal and non-stomatal conductance, and O_3 mole fraction were considered as fixed factors in 3 separate ANOVA tests and assigned at 2 levels ("high" and "low") by comparing the monthly means recorded in correspondence of the F_{TotO3} peak to the median of all the monthly mean values considered. The identification of the factors responsible for short-time variability (day-to-day and hourly variability) of F_{TotO3}, g_{StomO3}, and $g_{NonStomO3}$ was made with a backward stepwise regression on the daily means and half-hourly values (not-gapfilled data) of the summer seasons. All the analysis was performed with Statistica 12.0 software (Statsoft Inc., USA).

Results

Climatic conditions

Table S1 describes the climatic conditions of the different seasons during the 7 years of measurements. These data will be a useful reference when discussing the results.

The year 2013 was characterized by the coldest, most humid and rainy spring; 2014 exhibited the coldest and most rainy summer; 2015 was dry and arid, in both spring and summer, with the lowest soil water content (SWC) values; 2017, as 2015, had a quite arid spring, but it was followed by a cool and humid summer; 2018 had the summer with the highest soil water availability and a spring with the lowest O_3 mole fractions; 2019, after a spring with the highest levels of soil water availability, presented the hottest and most arid summer, which was also characterized by the highest O_3 mole fractions; finally, 2020 showed the hottest and most arid spring, followed by a summer with the lowest mean O_3 mole fraction among the 7 considered summers.

O_3 fluxes

An overview of all the deposition fluxes, as well as their partition into stomatal (F_{StomO3}) and non-stomatal ($F_{NonStomO3}$) components, is reported in **Figure 2**. The ANOVA test on the monthly averages of F_{TotO3} for all the 7 years (**Figure 2a**) highlighted a certain interannual variability of the total O_3 deposition when the year is used as a grouping factor for the test ($P = 0.088$, n.s.). However, the difference in the monthly average of F_{TotO3} between the two most contrasting years, that is, the years with the highest and the lowest annual peak of F_{TotO3} (2018 and 2020), was significant at a paired *t* test ($P = 0.004$), although the sample size was relatively small ($n = 24$). This variability was mainly driven by the stomatal component of the flux: when the annual peak of the stomatal flux was high, the peak of the total flux was also high (e.g., year 2018: $F_{StomO3} = 7.51 \pm 0.26$ and $F_{TotO3} = 11.92 \pm 0.38$ nmolO_3 m^{-2} s^{-1}), and when the annual peak of the stomatal flux was low, the annual peak of the total flux was also low (e.g., year 2020: $F_{StomO3} = 3.48 \pm 0.13$ and $F_{TotO3} = 6.36 \pm 0.20$ nmolO_3 m^{-2} s^{-1}). On the contrary, the annual peak of the $F_{NonStomO3}$ showed a much lower variation over the years, ranging between 2.87 ± 0.12 nmolO_3 m^{-2} s^{-1} of July 2020 and 4.41 ± 0.23 nmolO_3 m^{-2} s^{-1} of July 2018 (**Figure 2a**). The average diurnal cycle of the F_{StomO3} showed a marked seasonal variation (**Figure 2b**), with the average daily peak ranging from a minimum of 0.93 ± 0.09 nmolO_3 m^{-2} s^{-1} in January (1:00 pm) to a maximum of 8.89 ± 0.33 nmolO_3 m^{-2} s^{-1} in July (1:00 pm), while the non-stomatal flux showed a lower diurnal variation in the different months, with the average daily peak ranging from a minimum of 2.7 ± 0.24 nmolO_3 m^{-2} s^{-1} in December to a maximum of 4.43 ± 0.36 nmolO_3 m^{-2} s^{-1} in July.

Stomatal fraction and effect of the different flux-partition approaches

The comparison of the 3 different flux-partition approaches was made on the dry canopy data for 2018, when H_2O flux measurements below canopy were fully available. Moreover, 2018 was the year that showed the highest stomatal fluxes of both O_3 and H_2O. Below canopy measurement of LE fluxes are useful for estimating the fraction of water evaporated from the soil, a fraction that should be subtracted from the LE measured above the

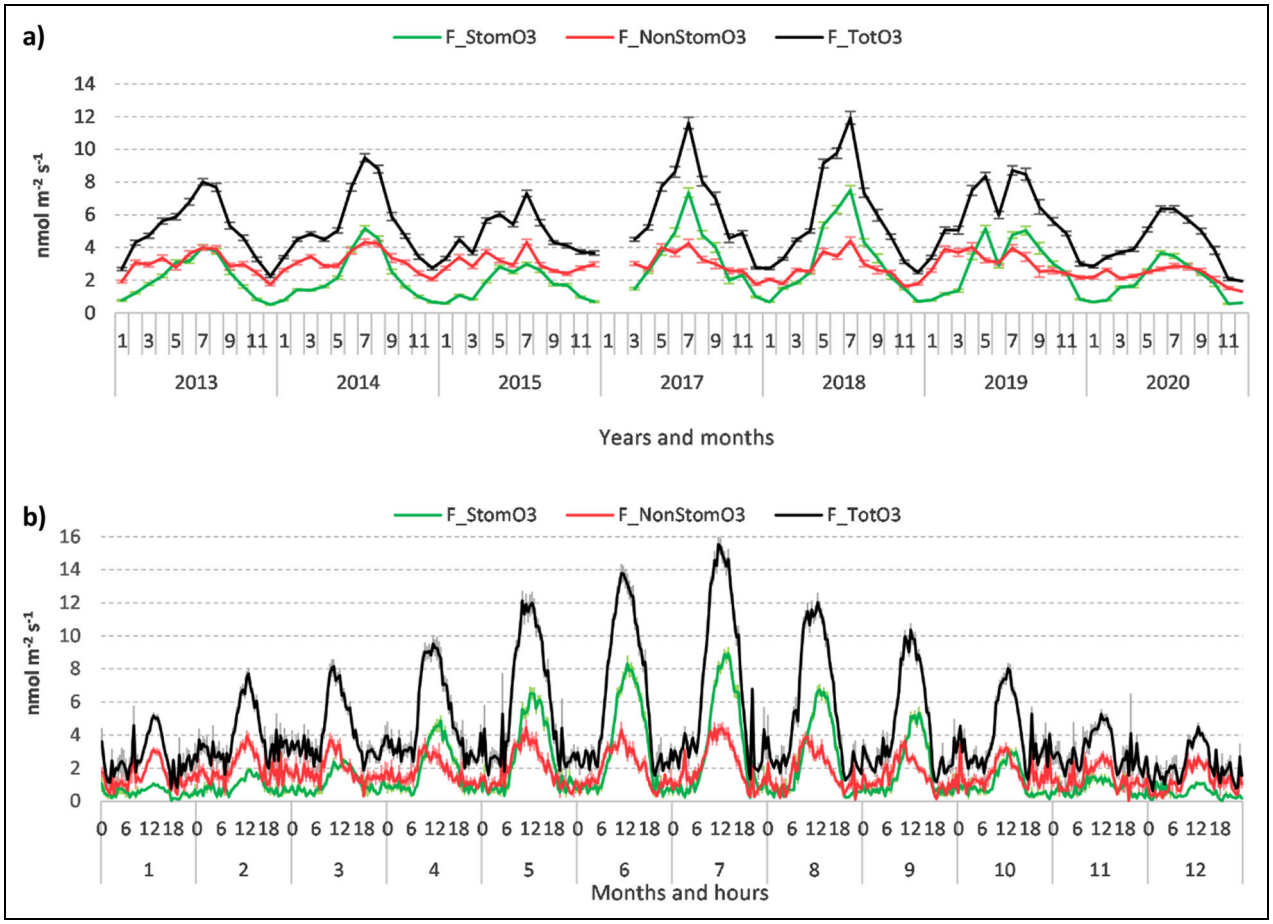

Figure 2. An overall view. (a) Monthly averages of O_3 fluxes in the 7-year campaign. (b) Average year: mean daily cycles of total O_3 deposition fluxes (F_TotO3), stomatal (F_StomO3) and non-stomatal (F_NonStomO3) O_3 fluxes in the different months. Vertical bars represent the standard error of the mean.

canopy to avoid attributing this amount of water to stomatal transpiration, thus leading to an overestimation of the stomatal fluxes in the partition process. The application of the approach developed by Lamaud et al. (2009) resulted in a good linear relationship between the stomatal conductance to O_3 (g_{StomO3}) and the CO_2 assimilation flux (A), $g_{StomO3} = \alpha \cdot A$, with $\alpha = 19$ cm s^{-1}/mmol $m^{-2}s^{-1}$ and $R^2 = 0.93$. The g_{StomO3} calculated from nonnegative A values resulted in the stomatal flux reported in **Figure 3a** (blue line), which in summer months was lower than the same flux calculated with the classic Penman–Monteith approach (green line). This difference reflects the fact that the Penman–Monteith approach may not completely exclude the non-stomatal water-vapor flux, that is, the water flux from soil, while the Lamaud's approach explicitly excludes it because it is based on the analysis of the CO_2 fluxes. Furthermore, it should be remembered that the Lamaud's methodology was developed for maize canopies where the effect of soil evaporation is less relevant than in forests, because maize canopy is denser and more closed. Nonetheless, during the rest of the year, the 2 approaches were fairly in agreement.

For the application of the third approach, we started from the observation that regardless of the season, the below-canopy water fluxes were well correlated with the above-canopy water fluxes ($LE_{below} = \beta\ LE_{above}$), with a proportionality coefficient $\beta = 0.1991$ and $R^2 = 0.86$. Hence, we assumed that $(1 - \beta) \cdot LE_{above}$ was the LE quota due to the canopy transpiration, and we used it also for the partition process of all the other years. The resulting stomatal flux for the comparison year is shown in **Figure 3a** (red line). The estimation with this method is in agreement with that obtained with the approach of Lamaud et al. (2009) for most of the year (+1.2% on average, with respect to the Lamaud's approach), even though it showed slightly higher differences in the midday hours of July (+17.1%) and August (−17.2%).

Figure 3b shows that in the daylight hours, the stomatal fraction of the total deposition was on average 16.4% lower than the fraction estimated with the Penman–Monteith inversion (the first approach), and it ranged between 20% and 60% of the total O_3 deposition, with an average value of 42.6% for the whole year and 52% for the spring and summer seasons. It is worth noting that despite the high interannual variability of the F_{TotO3} shown in **Figure 2a**, the stomatal fraction was similar throughout the 7 years. In fact, the maximum fraction of O_3 absorbed by the canopy crowns was on average 60% of the total O_3 deposition on the forest (**Figure 3b**), regardless the total amount of O_3 received by the ecosystem in the different years (compare for example 2018 vs. 2020, 2 years with very different total O_3 fluxes).

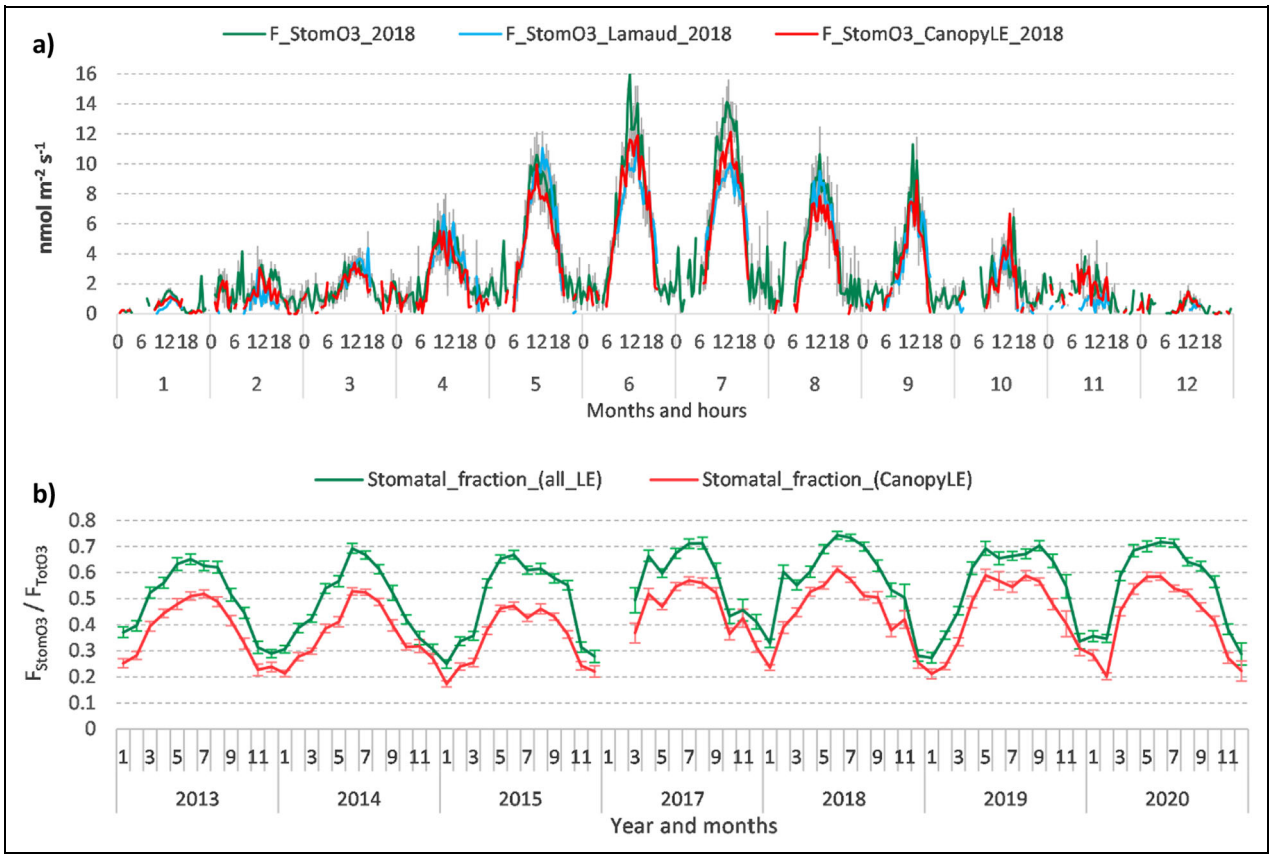

Figure 3. Effect of the different partition approaches. (a) Comparison of the stomatal fluxes derived with the 3 partition approaches in 2018 (cfr the Methodology section for details). Mean daily cycle of O_3 stomatal fluxes in the different months. (b) Comparison of the stomatal fraction of O_3 deposition obtained with the first and the third partition approach. The daytime (08:00–18:00) monthly averages are presented for the 7 years. Stomatal_fraction_(all_LE) refers to the partition made with the evapotranspiration measured above the canopy (LE) while Stomatal_fraction_(CanopyLE) refers to the partition made with the crown transpiration only (i.e., the measured top canopy LE minus the measured below canopy LE). Vertical bars represent the standard error of the mean.

Effect of the storage

The O_3 storage represents a temporary accumulation of O_3 in the air column below the EC measuring point or a temporary O_3 release out of the same air column, and it does not necessary represent a true O_3 removal or production at the target surface. The effect of the storage is reported in **Figure 4**, which presents a comparison between the total deposition fluxes obtained by considering (blue line) or not considering (black line) the storage flux. The effect of the storage caused an increase of the evening deposition fluxes during the vegetative months that could be due to the decrease of the O_3 mole fractions occurring in those hours, because O_3 production was no longer supported by photochemistry, and physical deposition or chemical consumption processes on surfaces tended to prevail. However, in the morning hours, when O_3 mole fractions increase and nitric oxide (NO) mole fractions below canopy are relatively high (**Figure 4**, yellow line), the storage correction could not fully represent the real deposition flux occurring in those hours, since for a reactive species like O_3 some of the stored gas may be destroyed within the canopy by NO titration and potentially by reaction with BVOCs, slowing down the O_3 mole fraction increase observed in the morning.

Conductances and deposition velocities

The deposition velocities ($Vdep_{O3}$) illustrated in **Figure 5a** and **b** showed a similar mean diurnal course in spring, summer, and autumn, with a peak between 5.2 ± 0.2 mm s^{-1} (summer) and 6.7 ± 0.4 mm s^{-1} (autumn) at 10:00 am. On the other hand, in winter $Vdep_{O3}$ was on average almost doubled, and the mean diurnal course showed a peak of 17.8 ± 4.4 mm s^{-1} in the early morning hours (07:00 am).

The diurnal course of g_{StomO3} (**Figure 5c**), averaged over the 7 years, was surprisingly similar in all the 4 seasons, with a maximum value around 3.5 mm s^{-1}. Only a slightly different diurnal shape and a greater uncertainty in autumn and winter can be observed. Nonetheless, the summer diurnal course showed an interannual variability that matches the interannual variability of both total and stomatal O_3 fluxes (**Figure 5d**). The highest and lowest values were recorded in 2018 and 2015, respectively. These

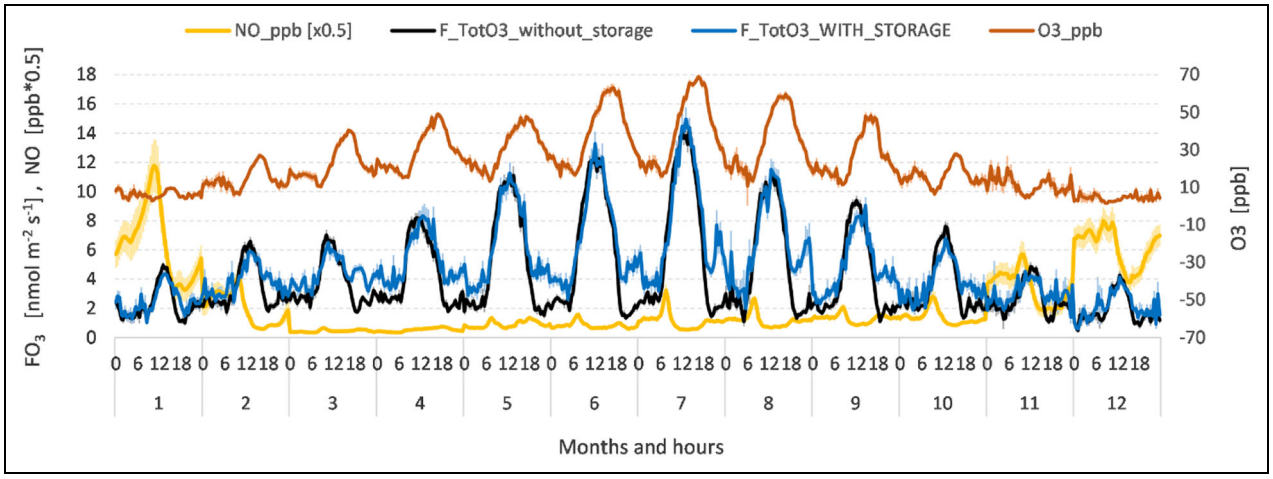

Figure 4. Effect of the storage correction on the total and non-stomatal O_3 fluxes. Comparison of the total O_3 deposition fluxes corrected and not corrected for storage. The mean daily cycles of O_3 fluxes (F_TotO3), nitric oxide (NO) and O_3 mole fractions in the different months, averaged over the 7 years, are presented. Vertical bars represent the standard error of the mean.

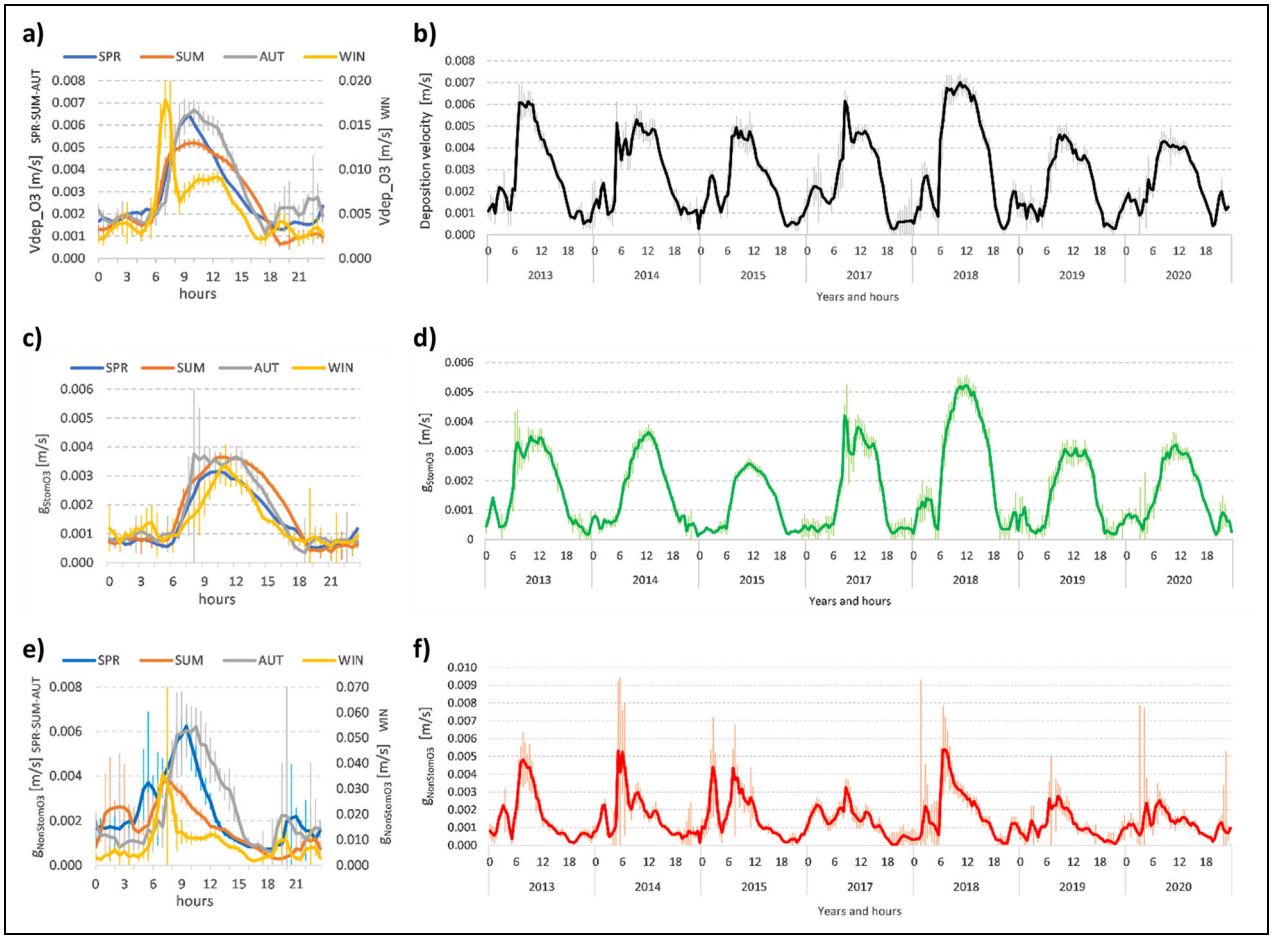

Figure 5. Ozone deposition velocity, stomatal, and non-stomatal conductances. (a) Mean daily cycle of O_3 deposition velocity in the 4 seasons of the 7 years of measurements. (b) Interannual variation of summer deposition velocity. Mean summer daily cycles are presented. (c) Mean daily cycle of stomatal conductance in the 4 seasons of the 7 years of measurements. (d) Interannual variation of summer stomatal conductance. Mean summer daily cycles are presented. (e) Mean daily cycle of non-stomatal conductance in the 4 seasons of the 7 years of measurements. (f) Interannual variation of summer non-stomatal conductance. Mean summer daily cycles are presented. Vertical bars represent the standard error of the mean.

2 years were also characterized by the highest (year 2018) and lowest (year 2015) SWC in summer.

The non-stomatal conductance to O_3 ($g_{NonStomO3}$) is reported in **Figure 5e** and **f**. The diurnal cycle showed an early morning peak both in summer and winter, even though in winter the peak was about one order of magnitude greater than in summer (**Figure 5e**). Then, in the afternoon, $g_{NonStomO3}$ declined to low values in all the seasons. The high mole fractions of NO in winter (cfr **Figure 4**, yellow line), particularly in the morning, suggest that the non-stomatal deposition in winter was linked to O_3 titration by the NO advected in the canopy without leaves.

The temporal alignment of the morning peak of $g_{NonStomO3}$ with the morning peak of NO mole fractions in the summer season suggests a similar process even for the growing season months, but with NO originated by soil as well described by Finco et al. (2018) for the same site. On the contrary, the $g_{NonStomO3}$ in the evening and in the night hours during the vegetative period showed values which are comparable with the typical values of the leaf cuticular resistance (0.4 mm s^{-1}, $R_{NonStom}$ = 2,500 s m^{-1} as from Emberson et al., 2000 and Simpson et al., 2012), once they have been rescaled according to the LAI, that is, between 0.1 mm s^{-1} and 0.58 mm s^{-1} ($R_{NonStom}$ between 1,000 and 1,700 s m^{-1}). Higher $g_{NonStomO3}$ values during the night were due to high humidity values or dew deposition (see next section). A summer interannual variability was also evident in **Figure 5f**. For example, in 2018, the summer mean diurnal cycles of $g_{NonStomO3}$ peaked at 5.5 ± 1.8 mm s^{-1} in the first hours of the morning, while in 2020, the peak diurnal value was halved, 2.5 ± 0.5 mm s^{-1}.

Drivers of half-hourly stomatal and non-stomatal deposition

The main drivers of the stomatal and non-stomatal deposition are showed in **Figures 6** and **7**, which are based on the analysis of binned half-hourly data. The stomatal uptake of O_3 was mainly driven by the SWC and by all those factors that affect the stomatal behavior (**Figure 6**). The increase of g_{StomO3} was directly related to soil water increase (**Figure 6a**) and inversely related to air dryness increase (**Figure 6b**), in both summer and winter. In summer, g_{StomO3} was around its average minimum value until SWC exceeds the threshold of 0.14 m^3_{H2O} m^{-3}_{soil}. In winter, the increase of g_{StomO3} required a higher SWC because the evergreen species of the understorey vegetation has a less developed rooting system compared to mature deciduous trees. The functional relationship between the SWC and g_{StomO3} proposed by the UNECE Mapping Manual (CLRTAP, 2017) for a broadleaf deciduous forest, and adopted by the DO_3SE model (as f_{SWC}), does not seem to describe adequately what was observed in our forest. However, a direct comparison between our data and the DO_3SE parameterization should be taken with caution, since our measurements come from a whole ecosystem with mostly adult trees, while the DO_3SE parameterization is based on leaf-level measurements mainly taken on young trees in mesocosms (e.g., Open Top Chambers). Moreover, the parameterization of f_{SWC} strongly depends on the soil type, and it should not be surprising that the thresholds of SWC below which g_{StomO3} starts to decrease (SWC_{max}) and reaches its minimum (SWC_{min}), vary among the different ecosystems. Nonetheless, in our forest ecosystem and with our soil type, the functional relationship of the DO_3SE model fits better for the summer months if the values 0.13 m^3 m^{-3} and 0.23 m^3 m^{-3} are assigned to SWC_{min} and SWC_{max}, respectively.

Regarding the relationship with vapor pressure deficit (VPD), in summer g_{StomO3} decreased exponentially as VPD increased above 1.2 kPa and remained around a constant value below this threshold, until VPD got close to zero, when air was close to saturated, and g_{StomO3} started to increase more than exponentially. The threshold of 1.2 kPa for VPD is similar to the value of 1.1 kPa suggested by the UNECE Mapping Manual (CLRTAP, 2017) for the beginning of stomatal closure in modeling exercises for this kind of vegetation. However, above a VPD of 3.1 kPa g_{StomO3} reached a minimum value of 1.26 mm s^{-1} (36% of g_{max}), a value which is greater than the value of 0.35 mm s^{-1} (10% of g_{max}) indicated by the UNECE. The g_{StomO3} showed a typical parabolic behavior, increasing with temperatures between 13°C and 18°C in summer (**Figure 6c**), showing an optimum around 23°C, and decreasing at higher values. The value of the optimum temperature is very close to that adopted by the DO_3SE model for Mediterranean broadleaf deciduous forest (22°C), as suggested by the UNECE (CLRTAP, 2017), but the minimum temperature of DO_3SE (0°C) appears to be appropriate only for the spring season in our case. Instead, the summer data show a better fit with the DO_3SE parameterization for the stomatal response to air temperature if the minimum temperature is set to 11°C, while keeping the optimum and maximum temperature to 23°C and 39°C, respectively.

Regarding the effect of O_3 (**Figure 6d**), in all the seasons g_{StomO3} tended to decline as O_3 mole fraction increased, but this was likely due to the co-occurrence of conditions that favor the stomatal closure. However, the negative effect of O_3 on stomata cannot be excluded, as shown by many authors in controlled experiments (Hoshika et al., 2012; Lombardozzi et al., 2012).

For the non-stomatal deposition (**Figure 7**), the negative relationship with mechanical (**Figure 7a**) and thermal turbulence (**Figure 7b**), as well as wind speed (data not shown), would exclude a deposition process based on the disruption of O_3 on leaf surface, which could be expected to increase at increasing wind speed and turbulence. The remarkable negative relationship with air temperature (**Figure 7c**) is probably the result of a temporal misalignment between the $g_{NonStomO3}$ daily cycle (**Figure 5e**) and the T daily cycle. The non-stomatal deposition, in fact, was higher when T was low and vice versa. This was related to the fact that in the first hours of the morning (characterized by low temperatures) NO mole fractions were high and O_3 removal by the chemical sink was also high. Thus, the negative relationship between $g_{NonStomO3}$ and air T does not exclude the thermal decomposition of O_3 on cuticles, barks, and nonliving surfaces.

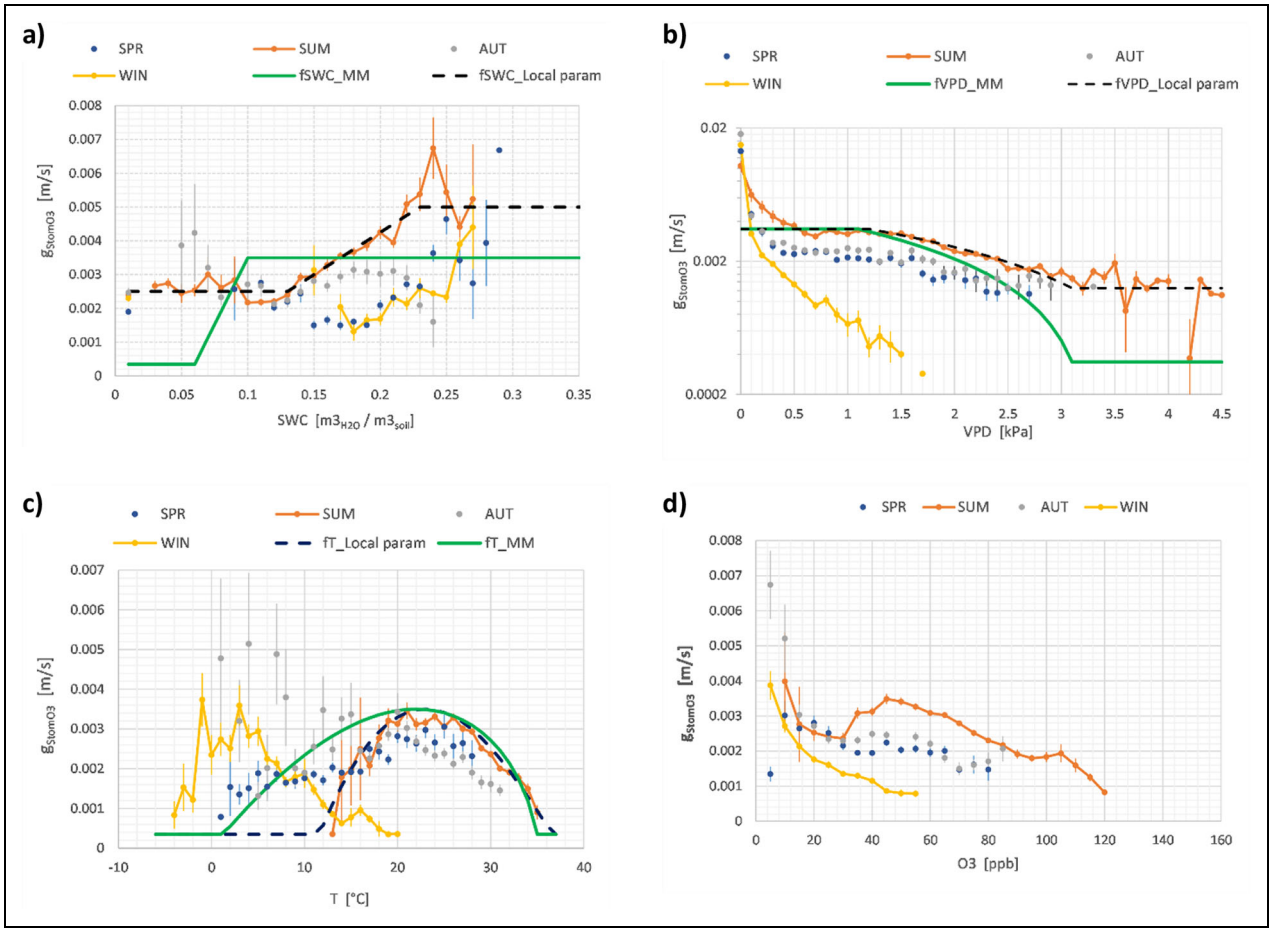

Figure 6. Drivers of half-hourly stomatal conductance. Seasonal relationships between stomatal conductance and (a) SWC, soil water content, (b) VPD, vapor pressure deficit (g_{StomO3} in log-scale), (c) T, air temperature, (d) O_3, ozone mole fraction. In graphs (a), (b), and (c), the green lines indicate the original functional relationships of the UNECE Mapping Manual (CLRTAP, 2017) for broadleaf deciduous forests, as adopted by the DO_3SE model (Emberson et al., 2000). The dashed black lines indicate the best fit of these functions for the summer season in our forest. Binned half-hourly data, each point represents the mean value of the bin. Vertical bars represent the standard error of the mean.

Instead, the non-stomatal deposition was driven by air humidity because $g_{NonStomO3}$ tended to rise with relative humidity (RH, **Figure 7d**) and exponentially decreased at increasing VPD (**Figure 7e**). The link between non-stomatal deposition and air humidity has been shown also by Altimir et al. (2004) and Lamaud et al. (2002). Even water on leaf and bark surfaces plays a role in non-stomatal deposition. **Figure 8** shows that the surface conductance to O_3 was higher when the canopy was wet compared to when it was dry (no dew on leaves and air temperature not higher than 2°C above dew temperature). This is particularly evident in autumn and winter. While in summer and spring the presence of water on the leaves reduced the cuticular conductance to O_3, as proposed by Zhang et al. (2002), in the other months (when broadleaf trees have senescent or no leaves at all), it is likely that the O_3 decomposition in water films is enhanced by the presence of soluble organic compounds in water, coming from senescent or dead vegetal material (Potier et al., 2017). On the contrary, the SWC did not influence the non-stomatal deposition in summer (**Figure 7f**) because in this season the canopy is closed and the soil has less influence on this deposition, while in winter soil water leads to a decrease of $g_{NonStomO3}$ because, when water fills the soil pores, the internal soil surface available for O_3 deposition decreases, as shown by Fumagalli et al. (2016).

Regarding the chemical sink, there was a general tendency for an increase of non-stomatal deposition at increasing NO mole fractions (**Figure 7g**), thus confirming what was already explained in the section about the effect of the storage (**Figure 3a**). The evidence of an O_3 chemical sink due to reaction with NO can also be seen in the relationship between the non-stomatal deposition and O_3 (**Figure 7h**). Two distinct regimes are evident in the graph, both in winter and in summer: a linear relationship below 20 ppb of O_3 mole fraction, and an exponential relationship above 20 ppb. The linear decline of $g_{NonStomO3}$ at increasing O_3 mole fractions below 20 ppb can be associated with O_3 reaction with NO, which occurs stoichiometrically 1:1. When O_3 mole fraction is above 20 ppb, the excess of O_3 leads to a slower exponential decline of $g_{NonStomO3}$ with increasing O_3. Again, looking at **Figure 7e**, it is worth noting that below VPD of 0.9 kPa, in summer nights (cross symbols), the non-stomatal

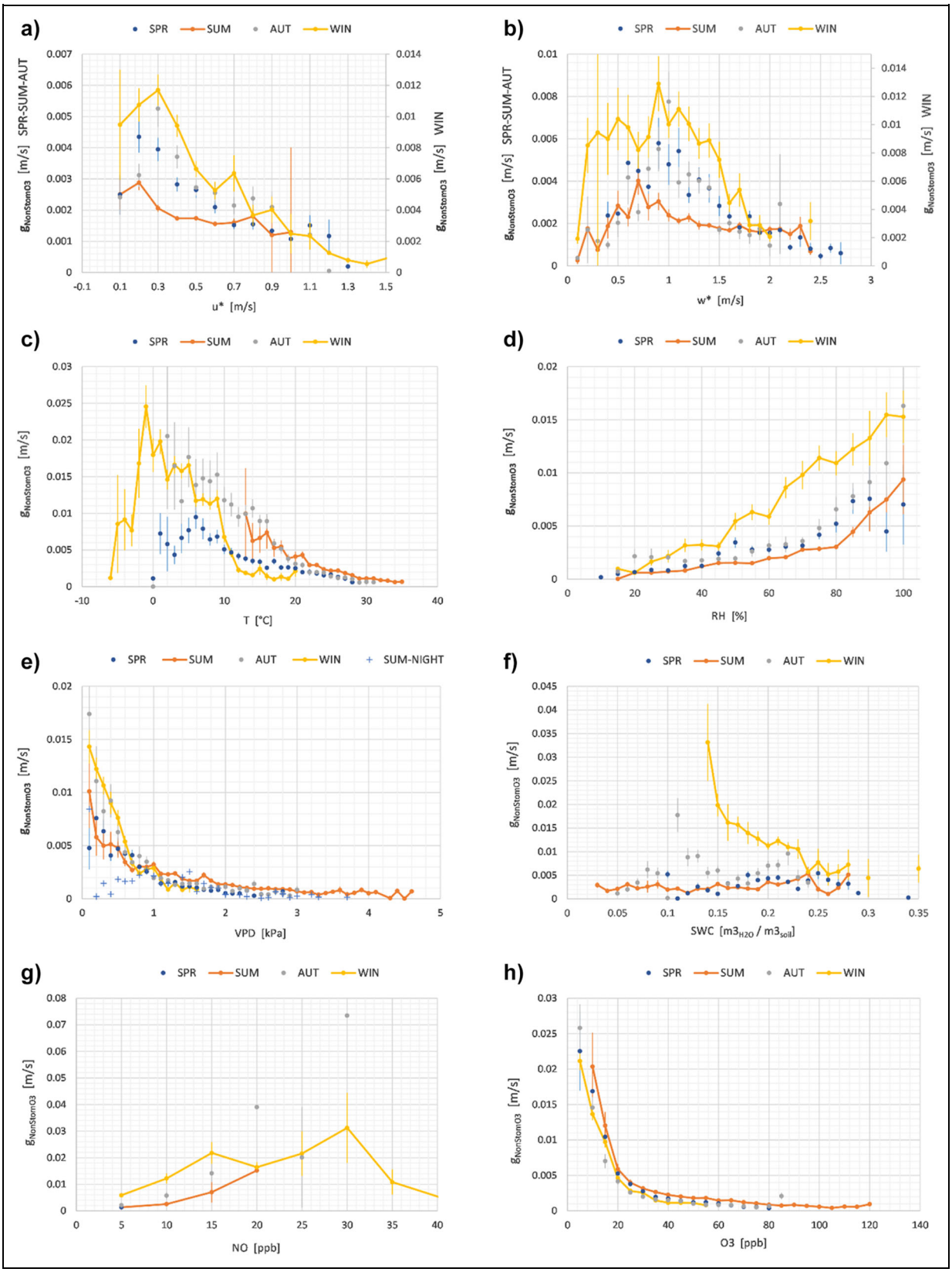

Figure 7. Drivers of the half-hourly non-stomatal conductance. Seasonal relationships between non-stomatal conductance and (a) u*, friction velocity, (b) w*, convective velocity, (c) T, temperature, (d) RH, relative humidity, (e) VPD, vapor pressure deficit, (f) SWC, soil water content, (g) NO, nitric oxide mole fraction, (h) O_3, ozone mole fraction. Binned half-hourly data, each point represents the mean value of the bin. Vertical bars represent the standard error of the mean.

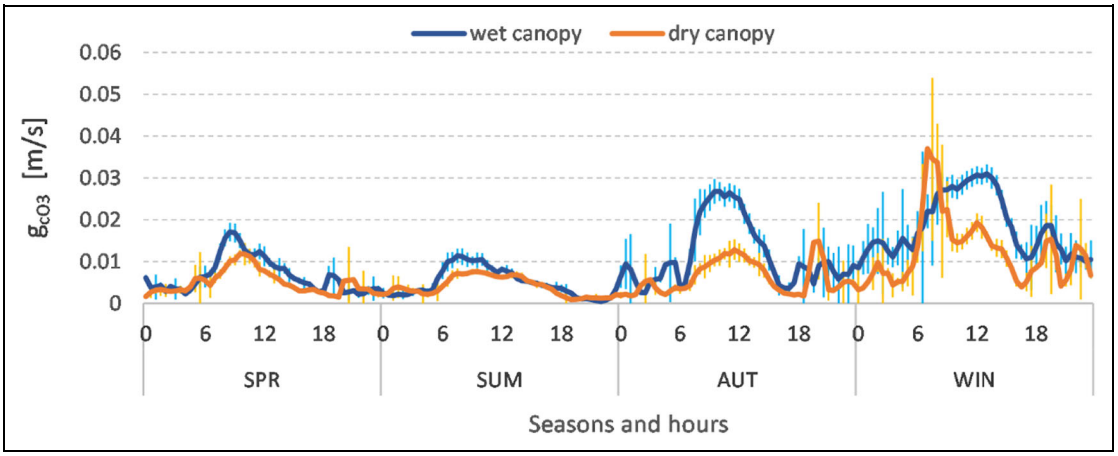

Figure 8. Drivers of the non-stomatal conductance. Seasonal mean daily cycle of the surface conductance (g_{C_O3}) with wet canopy and with dry canopy (air temperature up to 2°C above T_{dew}). Vertical bars represent the standard error of the mean.

deposition decreased when air gets closer to water saturation. This suggests that the greater non-stomatal deposition observed in daylight hours with VPD values below 0.9 kPa, that is, when stomata are fully open, is related to some chemical reactions with substances emitted by the stomata, likely BVOC and isoprene among others, as reported by Schallhart et al. (2016) for the same site.

Analysis of the temporal variability of summertime fluxes and its drivers

The analysis of the flux variability and its determinants at different time scales was focused only on the summer season, the season in which O_3 fluxes are maximum and the deciduous forest has uniform conditions of LAI. This could give more emphasis to the role of the stomatal component, as non-stomatal processes seem to dominate in other periods of the year.

Interannual variability

As shown in **Figure 2**, F_{TotO3} presented the maximum monthly mean value always in July for all the 7 years of measurements, regardless its magnitude. The 1-way ANOVA test between July monthly means and the corresponding g_{StomO3} (as fixed factor) monthly means subdivided in 2 dimensional classes (high values and low values) confirmed that the F_{TotO3} peak in July (i.e., the maximum monthly value for each year) is significantly influenced by g_{StomO3} ($P = 0.026$, $n = 7$). The same analysis performed on $g_{NonStomO3}$ or O_3 mole fraction as fixed factors (both at 2 levels) didn't show any statistically significant effect on the maximum annual peak of F_{TotO3} ($P = 0.222$ for $g_{NonStomO3}$, $P = 0.781$ for O_3 mole fraction, $n = 7$). In any case, the small sample size used for the test suggests some caution in generalizing these results until more multiannual measurements will became available.

Day-to-day variability

At a shorter time level, such as day-to-day and half-hourly scale, the number of the available summer data (June–July–August) enables using a stepwise regression method, which allows the simultaneous analysis of a large number of variables and the identification of the predictors subset that most adequately describes the variability at that level. This analysis highlighted that at a daily level, g_{StomO3} was a significant driver of the O_3 flux variability (while $g_{NonStomO3}$ was not), as evidenced by the backward stepwise regression ($R^2 = 0.42$), even though this method identifies also the O_3 mole fraction as a significant factor at this level (**Table 1a**). In turn, the day-to-day variability of g_{StomO3} was confirmed to be governed by SWC and the daily mean value of VPD, with the addition of PAR, although the predictivity of the obtained regression model was low ($R^2 = 0.28$).

Instead, the determinants of the day-to-day variability of $g_{NonStomO3}$ were the mean air temperature and turbulence (u*), both inversely correlated to $g_{NonStomO3}$, as well as the soil temperature which can be considered as a descriptor of the seasonal climatic evolution because it varies gradually during the season. However, when the backward stepwise regression included the daily average NO mole fraction (available only from 2018), the model identified this latter factor as the only determinant of $g_{NonStomO3}$ (**Table 1a**, last column), although the overall predictivity was still very low ($R^2 = 0.15$).

Half-hourly variability

At a shorter time scale (**Table 1b**), both g_{StomO3} and $g_{NonStomO3}$ together with O_3 mole fraction were selected by the stepwise procedure as significant descriptors of the half-hourly O_3 flux in the summer season ($R^2 = 0.35$). The predictors of the half-hourly g_{StomO3} variability were the same already identified for the daily time scale, with the addition, however, of RH, T_{air}, and u* ($R^2 = 0.32$). Regarding the half-hourly $g_{NonStomO3}$ variability, air temperature and humidity (T_{air}, RH) were added to the only predictor selected for the daily scale, that is, the NO hourly mole fraction (**Table 1a**, last column).

It is worth noticing that the stepwise regression models confirmed, for the selected drivers, the directions (positive or negative) of the relationships with g_{StomO3} and

Table 1. Backward stepwise regression on summer data

(a) Diurnal daily means, summer

		Dependent Variable									
		F_{TotO3}		F_{TotO3}		g_{StomO3}		$g_{NonStomO3}$		$g_{NonStomO3}$ (§)	
Regression	**Predictors**										
Test 1	$g_{NonStomO3}$	out	n.s.	—		—		—		—	
	g_{StomO3}	0.662	***	—		—		—		—	
	O_3	0.389	***								
Test 2	O_3	—		0.307	***	out	n.s.	out	**	out	
	VPD	—		−0.602	***	−0.509	***	out	*	out	**
	Tsoil	—		0.227	***	out	n.s.	0.189	***	out	
	SWC	—		0.352	***	0.208	***	out	*	out	
	Rainfall	—		out	n.s.	out	n.s.	out	n.s.	out	
	PAR	—		0.357	***	0.201	***	out	n.s.	out	
	RH	—		out	n.s.	out	n.s.	out	n.s.	out	
	Tair	—		out	n.s.	out	n.s.	−0.345	***	out	
	u*	—		out	n.s.	out	n.s.	−0.182	***	out	*
	Windspeed	—		out	n.s.	out	n.s.	out	n.s.	out	
	NO	—		—		—		—		0.39	***
	R^2	0.42		0.35		0.28		0.11		0.15	

(b) Half-hourly measurements, summer

		Dependent variable									
		F_{TotO3}		F_{TotO3}		g_{StomO3}		$g_{NonStomO3}$		$g_{NonStomO3}$ (§)	
Regression	**Predictors**										
Test 1	$g_{NonStomO3}$	0.221	***	—		—		—		—	
	g_{StomO3}	0.505	***	—		—		—		—	
	O_3	0.366	***								
Test 2	O_3			0.336	***	out	**	−0.328	***	out	n.s.
	VPD	—		−0.674	***	0.757	***	0.773	***	out	*
	Tsoil	—		out	**	out	n.s.	0.088	***	out	n.s.
	SWC	—		0.184	***	0.176	***	out	n.s.	out	n.s.
	Rainfall	—		out	n.s.	out	n.s.	out	n.s.	Out	n.s.
	PAR	—		0.452	***	0.244	***	0.107	***	Out	**
	RH	—		out	n.s.	0.962	***	0.658	***	0.227	***
	Tair	—		0.17	***	−0.448	***	−0.420	***	−0.124	***
	u*	—		0.112	***	0.160	***	−0.093	***	out	n.s.
	Windspeed	—		out	**	out	n.s.	out	n.s.	out	*
	NO	—		—		—		—		0.255	***
	R^2	0.35		0.46		0.32		0.20		0.21	

Standardized coefficients of the predictors included in the relationships found by the stepwise regression procedure to model the dependent variables in column. (§) Regression analysis including nitric oxide (NO) mole fraction when available. The status "out" denotes predictors that were excluded in the final model by the stepwise regression method. Predictors indicated with "—" were not included in the analysis. The statistical significance is indicated with stars: *** $P < 0.001$; ** $P < 0.01$; * $P < 0.05$; n.s. $P > 0.05$. Upper table (a) reports the results of the analysis performed on the diurnal daily means (day-to-day variability), while the lower table (b) show the same analysis performed on the half-hourly not-gapfilled measurements. The test 1 regressions use conductances as predictors. The test 2 regressions use all the agrometeorological factors that can influence conductances and fluxes as predictors.

Table 2. Ozone risk assessment: Estimated % of growth reduction for total biomass and root biomass in the 7 years (cfr UNECE Mapping Manual 2017 for details; CLRTAP, 2017)

Forest Type	Variable	Unit	2013	2014	2015	2017	2018	2019	2020	Mean
	POD1 (April 1 to September 30)	mmol m^{-2} PLA	8.76	10.05	7.11	12.47	14.83	12.79	7.84	10.55
Mediterranean deciduous oaks	Total biomass	% reduction	2.35	2.77	***1.83***	3.54	**4.30**	3.64	2.06	2.93
Mediterranean deciduous oaks	Root biomass	% reduction	3.31	3.89	***2.57***	4.98	**6.04**	5.13	2.90	4.12
Continental forests	Total biomass	% reduction	5.72	6.63	***4.57***	8.33	**9.99**	8.55	5.08	6.98

Bold italics numbers represent the minimum of the 7 years, and bold underlined numbers represent the maximum of the 7 years. PLA = projected leaf area.

$g_{NonStomO3}$ already found in the previous section, both on the half-hourly and daily time scale. The only exception was the VPD, which on a half-hourly scale was positively correlated with g_{StomO3} (**Table 1b**) while, instead, g_{StomO3} is expected to decrease at increasing VPD. This apparent contradiction is explained by the fact that, on the half-hourly time scale, the diurnal course of VPD is the same as the course of g_{StomO3}, that is, VPD is high around midday exactly when g_{StomO3} tends to be maximum, and vice versa. In fact, when the half-hourly variability was removed from the analysis and only the daily averages were considered, VPD was inversely related to g_{StomO3} (**Table 1a**) as expected.

Interannual variability of POD1 and effects on biomass growth

The phytotoxic O_3 dose above a threshold of 1 nmolO_3 m^{-2} s^{-1} for the whole ecosystem ($POD1_{ECOSYS}$; Table S1) showed a remarkable interannual variability, ranging from a minimum of 17.77 mmolO_3 m^{-2} (year 2015) to a maximum of 37.08 mmolO_3 m^{-2} (year 2018), with an annual average of 26.37 mmolO_3 m^{-2}. Considering on average a canopy LAI of 2.5 m^2 m^{-2} between April and October (**Figure 1**), the abovementioned annual average is equivalent to a POD1 of 10.55 mmol m^{-2}, for m^2 of projected leaf area (PLA; **Table 2**). Since the dose–response relationships available for forest trees are based on POD1 values referred to LAI = 1, the annual values of POD1 can be used to estimate an annual growth rate reduction of the total biomass ranging between 1.83% and 4.30% (2.93% on average over the 7 years) if this forest is considered as a Mediterranean deciduous oak forest, or between 4.57% and 9.99% (6.98% on average) if it is considered as a continental forest (Table 2).

Discussion

Ozone deposition fluxes

Few papers have dealt with O_3 deposition over a temperate deciduous forest such as Bosco Fontana. The summer daily course of $Vdep_{O3}$ observed at Bosco Fontana (**Figure 5a**) was slightly lower than those reported by Clifton et al. (2017), who showed the average daily courses of $Vdep_{O3}$, measured in summer from 1990 to 2000 at the Harvard Forest (USA). Clifton et al. (2017) reported summer daily peaks of $Vdep_{O3}$ between 5.0 ± 0.4 mm s^{-1} and 10.0 ± 1.0 mm s^{-1} while at Bosco Fontana the daily peaks were between 4.3 ± 0.4 mm s^{-1} and 7.0 ± 0.4 mm s^{-1} (**Figure 5b**). Furthermore, Finkelstein et al. (2000) and Visser et al. (2021) reported average daily peaks of the $Vdep_{O3}$ between 8.0 ± 0.2 mm s^{-1} and 10.0 ± 0.1 mm s^{-1} for mixed temperate forests. Deposition velocities in winter were remarkably higher than in summer (**Figure 5a**) with a peak value of 17.8 ± 4.4 mm s^{-1} in the early hours of the day. The winter enhancement of deposition velocity is related to an increase of NO mole fractions, air humidity, and surface wetness in that season, all factors that favor O_3 removal by non-stomatal processes, as described below.

The average daily peak of canopy conductance (g_{cO3}) observed at Bosco Fontana in summer (**Figure 8**) was 7.1 ± 1.1 mm s^{-1} for the case of a dry canopy, and 11.4 ± 1.7 mm s^{-1} for the case of a wet canopy. These values are comparable to the value of 10.0 ± 0.3 mm s^{-1} reported by Clifton et al. (2017) for the average daily peak of g_{cO3}, without any distinction between dry and wet canopy. A g_{cO3} daily peak of 12.0 ± 0.5 mm s^{-1} (averaged over 3 years of measurements) was instead reported by Visser et al. (2021) for a deciduous forest in northern Italy.

Stomatal conductance

The average daily peak of g_{StomO3} recorded in summer at Bosco Fontana (3.6 ± 0.2 mm s^{-1}; **Figure 5c**) was lower than those reported by Hogg et al. (2007), 4.5 ± 0.2 mm s^{-1} for a mixed temperate forest, and Visser et al. (2021), 7.0 ± 2.0 mm s^{-1} for a deciduous forest. Nonetheless, these differences are not surprising since stomatal conductance is strongly dependent on climatic conditions and particularly on the water availability in the soil. At Bosco Fontana, in fact, the g_{StomO3} was governed mainly by the SWC, but also by the air dryness and temperature. The relationships found between g_{StomO3} and these factors are quite similar to those adopted and parameterized in the CLRTAP (2017) for the stomatal conductance models used to calculate the POD in the O_3 risk assessment procedures.

Nonetheless, considering these results, some adjustments of the threshold values adopted for the parameterization of temperate deciduous forests seem necessary.

The presence of nonnegligible stomatal flux at night and in the winter seems surprising. However, a significant nighttime g_{StomO3} was reported from direct leaf measurements in a Californian forest (Grulke at al., 2004), from sap-flow measurements in a Mediterranean ecosystem (Mereu et al., 2009), and from measurements made with soil impermeabilized lysimeter in crops (Resco de Dios et al., 2015). As highlighted by Fowler et al. (2009) and Cailleret et al. (2018) in their comprehensive reviews, these results complicate the simplistic view of day–night differences in O_3 sinks in vegetation, with implications for O_3 risk assessment for vegetation. The detection of winter stomatal flux, on the other hand, was probably due to the presence of a dense understorey layer composed largely of evergreen and semideciduous species, with a remarkably high LAI (2.5 m^2 m^{-2}) as reported by George et al. (2021) in their comparative study performed across 29 different forest sites in Europe. The understorey species were active also in autumn and winter during the central part of the day, as confirmed by the significant CO_2 assimilation fluxes recorded during those seasons (data not shown).

Non-stomatal conductance

In summer, the average daily peak of $g_{NonStomO3}$ at Bosco Fontana was 3.9 $\pm$ 0.7 mm s^{-1}, lower than the values reported by various authors for other forest ecosystems. For example, Hogg et al. (2007) found an average daily maximum around 14.5 $\pm$ 2.0 mm s^{-1} and Visser et al. (2021) around 5.0 $\pm$ 2.0 mm s^{-1}. In winter instead, $g_{NonStomO3}$ values were almost one order of magnitude higher than those detected in the other seasons (**Figure 5e**), providing evidence for a strong intra-annual variation of the non-stomatal deposition processes. Moreover, $g_{NonStomO3\ was}$ always greater than g_{StomO3} in the evening hours, when the deposition on cuticles was prevailing, or at night when there was a reaction of O_3 with the NO emitted from the soil, or, again, in the early hours of the morning when the O_3 dissolved on the dew deposited on the canopy. The importance of the O_3 scavenging by the NO emitted below canopy at our site has already been shown by Finco et al. (2018), who evaluated the magnitude of this non-stomatal deposition process in a 1-month long measurement campaign in summer. Similar results were also reported by other authors for other forest ecosystems (e.g., Walton et al., 1997; Dorsey et al., 2004). The role of high air humidity, dew, and surface wetness in the non-stomatal processes has been repeatedly described by Fuentes et al. (1992), Lamaud et al. (2002), Gerosa et al. (2009a), and by Altimir et al. (2004; 2006) and Potier et al. (2015) who also proposed an appropriate parameterization. The positive influence of air humidity and dew on the $g_{NonStomO3}$ has also been experimentally demonstrated by Sun et al. (2016) who, by artificially inducing stomata closure, showed that O_3 deposition on leaves increased at increasing RH.

Unlike Lamaud et al. (2002), who found that non-stomatal deposition was linked to impaction processes and air penetration into the canopy, no positive relationship with atmospheric turbulence was found in our case. Similar findings were reported by Gerosa et al. (2009a), who observed a slightly negative correlation between $g_{NonStomO3}$ and u^* in a maquis ecosystem. At Bosco Fontana, this result could be due to the co-occurrence of several factors that tend to favor O_3 destruction in conditions of low turbulence, such as the high levels of NO during the early daytime hours when u^* was low.

The role of temperature with respect to $g_{NonStomO3}$ contrasted with what reported by Coyle et al. (2009), Hogg et al. (2007), and Fowler et al. (2001), who showed a positive relationship between the $g_{NonStomO3}$ and air temperature. Those authors concluded that a process of thermal decomposition of O_3 took place on the leaf surfaces facilitated by epicuticle waxes, confirming some of the results obtained by Cape et al. (2009) in lab experiments with simulated leaf surfaces. However, at our site the relationship between air temperature and $g_{NonStomO3}$ was negative (**Figure 7c**), suggesting that this process could have been masked by other processes that contributed to reducing the $g_{NonStomO3}$ as the temperature increased.

The great intra-annual variation of the $g_{NonStomO3}$ can be explained as the result of the combined effect of the seasonal variation of NO mole fraction and air humidity in the trunk space. NO mole fraction, in fact, rises in winter due to the increase of residential heating and vehicular traffic, particularly in the early hours of the morning. Moreover, in winter, NO is more easily advected in the intra-canopy space from the nearby urban areas because of the absence of leaves on the trees, thus enhancing the O_3 scavenging process. Air humidity also rises in winter with values of RH always above 85% and often close to 100% because of the presence of fog. These conditions, together with the enhanced presence of wet surfaces, lead to an increase of the non-stomatal removal of O_3 (Altimir et al., 2004; Altimir et al., 2006; Gerosa et al., 2009a), even though O_3 mole fractions and vertical fluxes in this season are low.

Temporal variability of summertime fluxes

The interannual variability of O_3 fluxes could be generally attributed both to the high mole fractions of O_3 in some years compared to others, and to the variability of g_{StomO3} and $g_{NonStomO3}$. However, the ANOVA test performed on the F_{TotO3} means of July showed that the interannual variability of the summer O_3 fluxes at our site was significantly influenced by the g_{StomO3} alone, and in turn to its drivers. This is particularly evident by comparing the year 2018 with the other years. These results are partially in contrast to what Clifton et al. (2017) found for the Harvard Forest, where non-stomatal deposition seemed to drive the interannual variability of O_3 fluxes. Moreover, Clifton et al. (2017) and Rannik et al. (2012) did not find any strong relationships with meteorology at hourly or daily scales and concluded that the unexplained interannual variability was likely due to processes that may act at a longer temporal scales (seasonal and multiannual) which may escape their analysis. At Bosco Fontana, where g_{StomO3} seems to dominate the deposition in the spring

and summer months, the long-term variability seems related to the seasonal variation of air temperature and SWC (Table S1). These findings underline once more the importance of multiannual measurements, as remarked by Clifton et al. (2020), since only this kind of measurement can capture features that could be missed at shorter time periods.

On a daily scale, the most significant drivers of the summer F_{TotO3} were g_{StomO3} and O_3 mole fraction (**Table 1**), partially confirming the results of Clifton et al. (2019), who also found that the stomatal deposition significantly guided the day-to-day variability of summer O_3 deposition velocity at the Harvard Forest. However, the same authors reported that also the dry–cuticular deposition (a non-stomatal process) contributed to the day-to-day variability, while in our site the $g_{NonStomO3}$ component showed to be a significant driver only at half-hourly time scale (**Table 1b**).

Stomatal and non-stomatal component of the total O_3 flux

The average stomatal fraction of the O_3 flux at our site (42.6% for the whole year and 52% in summer) was higher than those detected in our previous works in other ecosystems, both agricultural (e.g., Gerosa et al., 2003; Gerosa et al., 2004) and forest (e.g., Gerosa et al., 2005; Gerosa et al., 2009a; Gerosa et al., 2009b). However, it is comparable to the values reported by Clifton et al. (2017) (41% over 24 h, with daytime maxima of 82%) and by Zona et al. (2014) (42% over 24 h, with daytime maxima of 77% in the summer period). Our summer values are also consistent with the stomatal fraction reported by Zhang et al. (2006) for the Kane deciduous forest (USA) in summer (between 50% and 55%), but well below the 65% of the temperate deciduous forest of Borden (USA), as it can be deduced from Fuentes et al. (1992). The stomatal fraction (F_{StomO3}/F_{TotO3}) was similar over the different years despite the significant interannual variability of the total O_3 fluxes, a result that was also highlighted by Rannik et al. (2012). Considering that this ratio did not vary too much during the 7 years, we may try to better characterize the non-stomatal processes partially investigated by Finco et al. (2018) and Nemitz et al. (2013) at our site. According to what was reported by those authors, 18% of the O_3 deposition was due to chemical reaction with intra-canopy NO in dry canopy conditions, while no more than 3% was due to reactions of O_3 with VOCs. Therefore, since on average 52% of the O_3 deposition occurs by stomatal uptake in summer, the remaining 27% of the non-stomatal deposition can be attributed, in dry canopy conditions, to the deposition on leaf cuticles, soil, and plant surface. However, this value could rise when air humidity is high, and the surfaces are wet.

Understanding the contribution of each non-stomatal deposition pathways remains an uncertain aspect in the characterization of O_3 removal dynamics in ecosystems (Clifton et al., 2020). However, our estimates represent an attempt to provide the relative weight of the non-stomatal deposition related to dry deposition on surfaces (soil and vegetation) and O_3 chemical reaction with other trace gases (NO_x and VOCs). Moreover, the application of flux correction for the O_3 storage effect was found to be important for the interpretation of the measurements, and in particular to carefully evaluate the exchange processes on the surfaces. Nonetheless, for reactive species such as O_3, this correction is still an approximation because it does not consider the chemical reactions that may occur in the intra-canopy space, which remains unsolved. For a more precise assessment of the influence of chemistry on storage, it is necessary to employ a model that simultaneously solves both the chemistry and the O_3 exchange. However, despite these drawbacks, the storage correction allowed us to separate the process of deposition on the cuticles from the other non-stomatal deposition processes.

Comparison between different flux-partition approaches

If on one hand our measurements confirmed that the contribution of non-stomatal processes to O_3 deposition on forests cannot be considered negligible, on the other hand they showed that the correct estimation of the stomatal deposition is still affected by the flux partition procedure adopted. In their extensive review, Clifton et al. (2020) remarked that the correct quantification of the stomatal uptake with the EC technique is strictly related to the availability of canopy skin temperature and reliable estimates of the canopy transpiration and water evaporation from vegetation and soil. In this regard, the comparison of different flux partition approaches performed in this study has shown that the simple approach based on the subtraction of a percentage of H_2O flux attributed to the soil, as also used by Clifton et al. (2017), can be interesting and easy to apply, provided that reliable measurements of evapotranspiration below canopy are available for a sufficiently long period to estimate the value of that percentage. In our study, this latter approach gave results not dissimilar to those obtained with the CO_2-based approach by Lamaud et al. (2009), and it was in agreement with other methods to estimate forest transpiration based on seasonal LAI evolution, such as those proposed by Wang et al. (2014) and Wei et al. (2017). The consideration of these aspects is crucial to avoid overestimations of the O_3 stomatal fraction and the O_3 effect on vegetation. In any case, increasing the set of measurements to include below canopy measurements, at least of H_2O fluxes, is encouraged.

Phytotoxical ozone dose and estimation of the effects on vegetation

Although the quantification of the stomatal uptake is important for estimating the O_3 removal from atmosphere, it also provides important information for the assessment of plant response to O_3 stress.

The stomatal uptake, in fact, determined the interannual variability of the POD1 values, since the POD1 was not always related to the mean O_3 mole fraction recorded during the growing seasons (spring and summer; Table S1). The marked interannual variability of POD1 (e.g., 2015 vs. 2018; Table S1) also highlights the need for

multiannual measurements in order to have a more reliable O_3 risk assessment for forest ecosystems. The annual average value of 10.55 $mmolO_3\ m^{-2}$ PLA was lower than the critical level for total biomass established by the UNECE for the protection of Mediterranean deciduous forests (14 $mmolO_3\ m^{-2}$ PLA for total biomass; CLRTAP, 2017) but slightly higher than the critical level for significant negative effects on roots biomass growth (10.3 $mmolO_3\ m^{-2}$ PLA; CLRTAP, 2017). If, on the other hand, we consider the critical level established for continental forests (5.7 $mmolO_3\ m^{-2}$ PLA for total biomass; CLRTAP, 2017), this limit was almost twofold exceeded. Although the effect of O_3 on total biomass growth may seem small (**Table 2**), these estimations confirm that O_3 is a persistent stress factor for this forest ecosystem. Furthermore, the growth rate reduction of root biomass resulting from lower translocation of photosynthates from the leaves to the roots transposes the negative effects on the vegetative restart of the following year, as also highlighted by Grulke and Heath (2020). We may predict that this abiotic stress affects the overall carbon balance and the NEE of the forest; however, this hypothesis could be confirmed with future data analysis.

Conclusions

A new multiannual dataset of O_3 flux measurements is now available to test and improve the parametrization of O_3 deposition models, and for the estimations of the interannual variability of tropospheric O_3 budget in global models. The long-term monitoring campaign performed on the temperate deciduous broadleaf forest of Bosco Fontana revealed a marked interannual and intra-annual variability of O_3 deposition that seemed to be dominated by the stomatal component. Therefore, the drivers that influence g_{StomO3} (mainly soil water availability and air dryness) were responsible for the variability of the total O_3 flux at day-to-day and interannual time scales. The measurements confirmed the relationships used in SVAT models (Soil-Vegetation-Atmosphere Transfer models), such as DO_3SE (CLRTAP, 2017), to describe the dependence of the g_{StomO3} on various environmental drivers and provide insights for adapting those parameterizations to deciduous temperate forests. The non-stomatal O_3 deposition was mainly driven by air humidity, surface wetness, and chemical sinks such as reaction of O_3 with NO, the latter being emitted by the forest soil in summer or transported into the trunk space from outside the forest in winter.

The assessment of the potential O_3 effects on plants, performed through the calculation of the phytotoxic stomatal dose (POD1) for the 7 years, suggests that O_3 may reduce the plants growth rate by $3\%\ yr^{-1}$, on average, with a serious threat to the carbon balance at ecosystem level. The marked interannual variability of POD1 highlighted the need for multiannual measurements for reliable O_3 risk assessment.

This work has shown the importance of using canopy transpiration for the estimates of g_{StomO3} in the O_3 flux partition process, instead of the raw evapotraspiration measurements (LE) performed above the forest canopy. It also showed the benefit of correcting the EC data for storage in order to identify the different deposition phenomena, in particular the deposition on leaf cuticles that occurred in the evening hours.

Data accessibility statement

The following datasets were generated:

- Dataset-1 containing the monthly data of O_3 fluxes and deposition velocity (storage corrected).
- Dataset-2 containing the hourly means of O_3 fluxes (storage corrected and not) averaged per each month over all years.
- Dataset-3 containing the hourly means of deposition velocity, conductances, and main meteorological parameters, averaged over the summer months per each year.

The datasets are uploaded in a single supplemental file.

Supplemental files

The supplemental files for this article can be found as follows:

Datasets 1–3. xlsx
Description of Supplementary Data. Docx
Table S1. Docx

Acknowledgments

The authors acknowledge the European FP7 Project ÉCLAIRE (Effects of Climate Change on Air Pollution Impacts and Response Strategies for European Ecosystems, Grant Number 282910).

The present research was co-funded by the Catholic University of the Sacred Heart in the framework of the D1 and D3.1 calls for proposals (Years 2013–2020).

The authors are grateful to the administration and the personnel of the State National Reserve of Bosco Fontana for their availability and continuous support.

Competing interests

No competing interests were identified.

Author contributions

Conception and design: GG.
Acquisition of data: GG, AF.
Analysis and interpretation of data: GG, RM.
Drafted and/or revised the article: All authors.
Approved the submitted version for publication: All authors.

References

Altimir, N, **Kolari, P**, **Tuovinen, JP**, **Vesala, T**, **Bäck, J**, **Suni, T**, **Kulmala, M**, **Hari, P.** 2006. Foliage surface ozone deposition: A role for surface moisture? *Biogeosciences* **2**: 1739–1793. DOI: http://dx.doi.org/10.5194/bgd-2-1739-2005.

Altimir, N, **Tuovinen, JP**, **Vesala, T**, **Kulmala, M**, **Hari, P.** 2004. Measurements of ozone removal by Scots pine shoots: Calibration of a stomatal uptake model

including the non-stomatal component. *Atmospheric Environment* **38**: 2387–2398.

Andreae, MO, **Acevedo, OC**, **Araùjo, A**, **Artaxo, P**, **Barbosa, CGG**, **Barbosa, HMJ**, **Brito, J**, **Carbone, S**, **Chi, X**, **Cintra, BBL**, **da Silva, NF**, **Dias, NL**, **Dias-Júnior, CQ**, **Ditas, F**, **Ditz, R**, **Godoi, AFL**, **Godoi, RHM**, **Heimann, M**, **Hoffmann, T**, **Kesselmeier, J**, **Könemann, T**, **Krüger, ML**, **Lavric, JV**, **Manzi, AO**, **Moran-Zuloaga, D**, **Nölscher, AC**, **Nogueira, DS**, **Piedade, MTF**, **Pöhlker, C**, **Pöschl, U**, **Rizzo, LV**, **Ro, CU**, **Ruckteschler, N**, **Sá, LDA**, **Sá, MDO**, **Sales, CB**, **Santos, RMND**, **Saturno, J**, **Schöngart, J**, **Sörgel, M**, **de Souza, CM**, **de Souza, RAF**, **Su, H**, **Targhetta, N**, **Tóta, J**, **Trebs, I**, **Trumbore, SE**, **van Eijck, A**, **Walter, D**, **Wang, Z**, **Weber, B**, **Williams, J**, **Winderlich, J**, **Wittmann, F**, **Wolff, S**, **Yáñez-Serrano, AM**. 2015. The Amazon Tall Tower Observatory (ATTO): Overview of pilot measurements on ecosystem ecology, meteorology, trace gases, and aerosols. *Atmospheric Chemistry and Physics* **15**(18): 10723–10776. DOI: http://dx.doi.org/10.5194/acp-15-10723-2015.

Ashmore, MR. 2005. Assessing the future global impacts of ozone on vegetation. *Plant, Cell and Environment* **28**: 949–964. DOI: http://dx.doi.org/10.1111/j.1365-3040.2005.01341.x.

Aubinet, M, **Vesala, T**, **Papale, D** eds. 2012. *Eddy covariance. A practical guide to measurement and data analysis*. The Netherlands: Springer. (Springer Atmospheric Sciences). DOI: http://dx.doi.org/10.1007/978-94-007-2351-1.

Bellumè, M, **Maugeri, M**, **Mazzucchelli, E**. 1998. *Due secoli di osservazioni meteorologiche a Mantova*. Milano, Italy: Edizioni CUSL: 124.

Boylan, P, **Helmig, D**, **Park, JH**. 2014. Characterization and mitigation of water vapor effects in the measurement of ozone by chemiluminescence with nitric oxide. *Atmospheric Measurements Techniques* **7**: 1231–1244.

Buker, P, **Feng, Z**, **Uddling, J**, **Briolat, A**, **Alonso, R**, **Braun, S**, **Elvira, S**, **Gerosa, G**, **Karlsson, PE**, **Le Thiec, D**, **Marzuoli, R**, **Mills, G**, **Oksanen, E**, **Wieser, G**, **Wilkinson, M**, **Emberson, LD**. 2015. New flux based dose–response relationships for ozone for European forest tree species. *Environmental Pollution* **206**: 163–174.

Cailleret, M, **Ferretti, M**, **Gessler, A**, **Rigling, A**, **Schaub, M.** 2018. Ozone effects on European forest growth—Towards an integrative approach. *Journal of Ecology* **106**(4): 1377–1389.

Campanaro, A, **Hardersen, S**, **Mason, F.** 2007. *Piano di Gestione della Riserva Naturale e Sito Natura 2000 "Bosco della Fontana."* Quaderni Conservazione Habitat, 4. Verona, Italy: Cierre Edizioni: 221.

Cape, JN, **Hamilton, R**, **Heal, MR.** 2009. Reactive uptake of ozone at simulated leaf surfaces: Implications for 'non-stomatal' ozone deposition. *Atmospheric Environment* **43**: 1116–1123.

Clifton, OE, **Fiore, AM**, **Massman, WJ**, **Baublitz, CB**, **Coyle, M**, **Emberson, L**, **Fares, S**, **Farmer, DK**, **Gentine, P**, **Gerosa, G**, **Guenther, AB**, **Helmig, D**, **Lombardozzi, DL**, **Munger, JW**, **Patton, EG**, **Pusede, SE**, **Schwede, DB**, **Silva, SJ**, **Sörgel, M**, **Steiner, AL**, **Tai, APK**. 2020. Dry deposition of ozone over land: Processes, measurement, and modeling. *Reviews of Geophysics* **58**: e2019RG000670. DOI: http://dx.doi.org/10.1029/2019RG000670.

Clifton, OE, **Fiore, AM**, **Munger, JW**, **Malyshev, S**, **Horowitz, LW**, **Shevliakova, E**, **Paulot, F**, **Murray, LT**, **Griffin, KL.** 2017. Interannual variability in ozone removal by a temperate deciduous forest. *Geophysical Research Letters* **44**: 542–552. DOI: http://dx.doi.org/10.1002/2016GL070923.

Clifton, OE, **Fiore, AM**, **Munger, JW**, **Wehr, R.** 2019. Spatiotemporal controls on observed daytime ozone deposition velocity over northeastern US forests during summer. *Journal of Geophysical Research: Atmospheres* **124**: 5612–5628.

Convention on Long-Range Transboundary Air Pollution. 2017. Chapter III of Manual on methodologies and criteria for modelling and mapping critical loads and levels and air pollution effects, risks and trends, in *Mapping critical levels for vegetation. UNECE Convention on Long-Range Transboundary Air Pollution*. Berlin, Germany: Umwelbundesamt. Available at https://www.umweltbundesamt.de/sites/default/files/medien/4292/dokumente/ch3-mapman-2017-10.pdf. Accessed 20 June 2021.

Coyle, M, **Nemitz, E**, **Storeton-West, R**, **Fowler, D**, **Cape, JN.** 2009. Measurements of ozone deposition to a potato canopy. *Agricultural and Forest Meteorology* **149**: 656–666.

Dorsey, JR, **Duyzer, JH**, **Gallagher, MW**, **Coe, H**, **Pilegaard, K**, **Weststrate, JH**, **Jensen, NO**, **Walton, S.** 2004. Oxidized nitrogen and ozone interaction with forests. I: Experimental observations and analysis of exchange with Douglas fir. *Quarterly Journal of the Royal Meteorological Society* **130**: 1941–1955.

Emberson, L. 2020. Effects of ozone on agriculture, forests and grasslands. *Philosophical Transactions of the Royal Society A* **378**(2183): 20190327. DOI: http://dx.doi.org/10.1098/rsta.2019.0327.

Emberson, L, **Ashmore, MR**, **Cambridge, HM**, **Simpson, D**, **Tuovinen, JP.** 2000. Modelling stomatal ozone flux across Europe. *Environmental Pollution* **109**: 403–413.

Fan, SM, **Wofsy, SC**, **Bakwin, PS**, **Jacob, DJ**, **Fitzjarrald, DR.** 1990. Atmosphere-biosphere exchange of CO_2 and O_3 in the central Amazon forest. *Journal of Geophysical Research* **95**: 16851–16864.

Fares, S, **Savi, F**, **Muller, J**, **Matteucci, G**, **Paoletti, E.** 2014. Simultaneous measurements of above and below canopy ozone fluxes help partitioning ozone deposition between its various sinks in a Mediterranean Oak Forest. *Agricultural and Forest Meteorology* **198**: 181–191.

Finco, A, **Coyle, M**, **Nemitz, E**, **Marzuoli, R**, **Chiesa, M**, **Loubet, B**, **Fares, S**, **Diaz-Pines, E**, **Gasche, R**, **Gerosa, G.** 2018. Characterization of ozone deposition to a mixed oak–hornbeam forest—Flux measurements

at five levels above and inside the canopy and their interactions with nitric oxide. *Atmospheric Chemistry and Physics* **18**: 17945–17961. DOI: http://dx.doi.org/10.5194/acp-18-17945-2018.

Finco, A, **Marzuoli, R**, **Chiesa, M**, **Gerosa, G.** 2017. Ozone risk assessment for an Alpine larch forest in two vegetative seasons with different approaches: Comparison of POD1 and AOT40. *Environmental Science and Pollution Research* **24**: 26238–26248.

Finkelstein, PL, **Ellestad, TG**, **Clarke, JF**, **Meyers, TP**, **Schwede, DB**, **Hebert, EO**, **Neal, JA**. 2000. Ozone and sulfur dioxide dry deposition to forests: Observations and model evaluation. *Journal of Geophysical Research* **105**(D12): 15365–15377. DOI: http://dx.doi.org/10.1029/2000JD900185.

Foken, T, **Wichura, B.** 1996. Tools for quality assessment of surface based flux measurements. *Agricultural and Forest Meteorology* **78**: 83–205.

Fowler, D, **Flechard, C**, **Cape, JN**, **Storeton-West, RL**, **Coyle, M.** 2001. Measurements of ozone deposition to vegetation quantifying the flux, the stomatal and non-stomatal components. *Water, Air and Soil Pollution* **130**: 63–74.

Fowler, D, **Pilegaard, K**, **Sutton, MA**, **Ambus, P**, **Raivonen, M**, **Duyzer, J**, **Simpson, D**, **Fagerli, H**, **Fuzzi, S**, **Schjoerring, JK**, **Granier, C**, **Neftel, A**, **Isaksenm, ISA**, **Laj, P**, **Maione, M**, **Monks, PS**, **Burkhardt, J**, **Daemmgen, U**, **Neirynck, J**, **Personne, E**, **Wichink-Kruit, R**, **Butterbach-Bahl, K**, **Flechard, C**, **Tuovinen, JP**, **Coyle, M**, **Gerosa, G**, **Loubet, B**, **Altimir, N**, **Gruenhage, L**, **Ammann, C**, **Cieslik, S**, **Paoletti, E**, **Mikkelsen, TN**, **Ro-Poulsen, H**, **Cellier, P**, **Cape, JN**, **Horvath, L**, **Loreto, F**, **Niinemets, U**, **Palmer, PI**, **Rinne, J**, **Misztal, P**, **Nemitz, E**, **Nilsson, D**, **Pryor, S**, **Gallagher, MW**, **Vesala, T**, **Skiba, U**, **Brueggemann, N**, **Zechmeister-Boltenstern, S**, **Williams, J**, **O'Dowd, C**, **Facchini, MC**, **de Leeuw, G**, **Flossman, A**, **Chaumerliac, N**, **Erisman, JW.** 2009. Atmospheric composition change: Ecosystems–atmosphere interactions. *Atmospheric Environment* **43**: 5193–5267.

Fuentes, JD, **Gillespie, TJ**, **den Hartog, G**, **Neumann, HH.** 1992. Ozone deposition onto a deciduous forest during dry and wet conditions. *Agricultural and Forest Meteorology* **62**: 1–18.

Fumagalli, I, **Gruening, C**, **Marzuoli, R**, **Cieslik, S**, **Gerosa, G.** 2016. Long-term measurements of NO_x and O_3 soil fluxes in a temperate deciduous forest. *Agricultural and Forest Meteorology* **228**: 205–216.

George, J-P, **Yang, W**, **Kobayashi, H**, **Biermann, T**, **Carrara, A**, **Cremonese, E**, **Cuntz, M**, **Fares, S**, **Gerosa, G**, **Grunwald, T**, **Hase, N**, **Heliasz, M**, **Ibrom, A**, **Knohl, A**, **Kruijt, B**, **Lange, H**, **Limousin, J-M**, **Loustau, D**, **Lukes, P**, **Marzuoli, R**, **Molder, M**, **Montagnani, L**, **Neirynck, J**, **Peichl, M**, **Rebmann, C**, **Schmidt, M**, **Serrano, FRL**, **Soudani, K**, **Vincke, C**, **Pisek, J.** 2021. Method comparison of indirect assessments of understory leaf area index (LAIu): A case study across the extended network of ICOS forest ecosystem sites in Europe. *Ecological Indicators* **128**: 107841.

Gerosa, G, **Ballarin-Denti, A.** 2003. Regional scale risk assessment of ozone and forests. *Developments in Environmental Science* **3**: 119–139.

Gerosa, G, **Cieslik, S**, **Ballarin-Denti, A.** 2003. Micrometeorological determination of time-integrated stomatal ozone fluxes over wheat: A case study in Northern Italy. *Atmospheric Environment* **37**: 777–788.

Gerosa, G, **Finco, A**, **Boschetti, F**, **Brenna, S**, **Marzuoli, R.** 2014. Measurements of soil carbon dioxide emissions from two maize agroecosystems at harvest under different tillage conditions. *The Scientific World Journal* **2014**: 141345. DOI: http://dx.doi.org/10.1155/2014/141345.

Gerosa, G, **Finco, A**, **Mereu, S**, **Marzuoli, R**, **Ballarin-Denti, A.** 2009a. Interactions among vegetation and ozone, water and nitrogen fluxes in a coastal Mediterranean maquis ecosystem. *Biogeosciences* **6**: 1783–1798.

Gerosa, G, **Finco, A**, **Mereu, S**, **Vitale, M**, **Manes, F**, **Ballarin-Denti, A.** 2009b. Comparison of seasonal variations of ozone exposure and fluxes in a Mediterranean Holm oak forest between the exceptionally dry 2003 and the following year. *Environmental Pollution* **157**: 1737–1744. DOI: http://dx.doi.org/10.1016/j.envpol.2007.11.025.

Gerosa, G, **Marzuoli, R**, **Cieslik, S**, **Ballarin-Denti, A.** 2004. Stomatal ozone uptake by barley in Italy. "Effective exposure" as a possible link between concentration- and flux-based approaches. *Atmospheric Environment* **38**: 2421–2432.

Gerosa, GA, **Vitale, M**, **Finco, A**, **Manes, F**, **Ballarin Denti, A**, **Cieslik, S.** 2005. Ozone uptake by an evergreen Mediterranean forest (*Quercus ilex*) in Italy. Part I: Micrometeorological flux measurements and flux partitioning. *Atmospheric Environment* **39**: 3255–3266. DOI: http://dx.doi.org/10.1016/j.atmosenv.2005.01.056.

Goldstein, AH, **McKay, M**, **Kurpius, MR**, **Schade, GW**, **Lee, A**, **Holzinger, R**, **Rasmussen, RA.** 2004. Forest thinning experiment confirms ozone deposition to forest canopy is dominated by reaction with biogenic VOCs. *Geophysical Research Letters* **31**: L22106. DOI: http://dx.doi.org/10.1029/2004GL021259.

Grantz, DA, **Zhang, XJ**, **Massman, WJ**, **Delany, A**, **Pederson, JR.** 1997. Ozone deposition to a cotton (*Gossypium hirsutum* L.) field: Stomatal and surface wetness effects during the California ozone deposition experiment. *Agricultural and Forest Meteorology* **85**: 19–31.

Grulke, NE, **Alonso, R**, **Nguyen, T**, **Cascio, C**, **Dobrowolski, W.** 2004. Stomata open at night in pole sized and mature ponderosa pine: Implications for ozone exposure metrics. *Tree Physiology* **24**: 1001–1010.

Grulke, NE, **Heath, RL**. 2020. Ozone effects on plants in natural ecosystems. *Plant Biology* **22**: 12–37.

Güsten, H, **Heinrich, G**, **Schmidt, RWH**, **Schurath, U.** 1992. A novel ozone sensor for direct eddy covariance measurements. *Journal of Atmospheric Chemistry* **14**: 73–84.

He, C, **Clifton, O**, **Felker-Quinn, E**, **Fulgham, SR**, **Juncosa Calahorrano, JF**, **Lombardozzi, D**, **Purser, G**, **Riches, M**, **Schwantes, R**, **Tang, W**, **Poulter, B**, **Steiner, AL.** 2021. Interactions between air pollution and terrestrial ecosystems: Perspectives on challenges and future directions. *Bulletin of the American Meteorological Society* **102**(3): E525–E538.

Hogg, A, **Uddling, J**, **Ellsworth, D**, **Carroll, MA**, **Pressley, S**, **Lamb, B**, **Vogel, C.** 2007. Stomatal and non-stomatal fluxes of ozone to a northern mixed hardwood forest. *Tellus Series B* **59**: 514–525.

Hoshika, Y, **Watanabe, M**, **Inada, N**, **Koike, T.** 2012. Ozone-induced stomatal sluggishness develops progressively in Siebold's beech (*Fagus crenata*). *Environmental Pollution* **166**: 152–156.

Lamaud, E, **Carrara, A**, **Brunet, Y**, **Lopez, A**, **Druilhet, A.** 2002. Ozone fluxes above and within a pine forest canopy in dry and wet conditions. *Atmospheric Environment* **36**: 77–88.

Lamaud, E, **Loubet, B**, **Irvine, M**, **Stella, P**, **Personne, E**, **Cellier, P.** 2009. Partitioning of ozone deposition over a developed maize crop between stomatal and non-stomatal uptakes, using eddy-covariance flux measurements and modelling. *Agricultural and Forest Meteorology* **149**: 1385–1396.

Le Morvan-Quéméner, A, **Coll, I**, **Kammer, J**, **Lamaud, E**, **Loubet, B**, **Personne, E**, **Stella, P.** 2018. Impact of parameterization choices on the restitution of ozone deposition over vegetation. *Atmospheric Environment* **178**: 49–65.

Lee, X, **Massman, W**, **Law, B**. 2004. *Handbook of micrometeorology: A guide for surface flux measurements and analysis*. Dordrecht, the Netherlands: Kluwer Academic Publisher.

Lin, M, **Horowitz, LW**, **Xie, Y**, **Paulot, F**, **Malyshev, S**, **Shevliakova, E**, **Finco, A**, **Gerosa, G**, **Kubistin, D**, **Pilegaard, K.** 2020. Vegetation feedbacks during drought exacerbate ozone air pollution extremes in Europe. *Nature Climate Change* **10**: 444–451.

Lombardozzi, D, **Levis, S**, **Bonan, G**, **Sparks, JP.** 2012. Predicting photosynthesis and transpiration responses to ozone: Decoupling modeled photosynthesis and stomatal conductance. *Biogeosciences* **9**: 3113–3130.

Longo, L. 2004. Clima, in Mason, F ed., *Dinamica di una foresta della Pianura Padana. Bosco della Fontana. Seconda edizione con Linee di gestione forestale. Rapporti Scientifici 1. Centro Nazionale Biodiversità Forestale Verona - Bosco della Fontana*. Mantova, Italy: Arcari Editore: 16–17.

Marzuoli, R, **Gerosa, G**, **Bussotti, F**, **Pollastrini, M.** 2019. Assessing the impact of ozone on forest trees in an integrative perspective: Are foliar visible symptoms suitable predictors for growth reduction? A critical review. *Forests* **10**: 1144.

Massman, WJ. 1998. A review of the molecular diffusivities of H_2O, CO_2, CH_4, CO, O_3, SO_2, NH_3, N_2O, NO, and NO_2 in air, O_2 and N_2 near STP. *Atmospheric Environment* **32**: 1111–1127.

Mereu S, **Gerosa G**, **Finco A**, **Fusaro L**, **Muys B**, **Manes F**. 2009. Improved sapflow methodology reveals considerable night-time ozone uptake by Mediterranean species. *Biogeosciences* **6**: 3151–3162.

Michou, M, **Laville, P**, **Serça, D**, **Fotiadi, A**, **Bouchou, P**, **Peuch, VH.** 2005. Measured and modeled dry deposition velocities over the ESCOMPTE area. *Atmospheric Research* **74**(1–4): 89–116.

Mikkelsen, TN, **Ro-Poulsen, H**, **Hovmand, MF**, **Jensen, NO**, **Pilegaard, K**, **Egeløv, AH**. 2004. Five-year measurements of ozone fluxes to a Danish Norway spruce canopy. *Atmospheric Environment* **38**: 2361–2371. DOI: http://dx.doi.org/10.1016/j.atmosenv.2003.12.036.

Moffat, AM, **Papale, D**, **Reichstein, M**, **Hollinger, DY**, **Richardson, AD**, **Barr, AG**, **Beckstein, C**, **Braswell, BH**, **Churkina, G**, **Desai, AR**, **Falge, E**, **Gove, JH**, **Heimann, M**, **Hui, D**, **Jarvis, AJ**, **Kattge, J**, **Noormets, A**, **Stauch, VJ.** 2007. Comprehensive comparison of gap-filling techniques for eddy covariance net carbon fluxes. *Agricultural and Forest Meteorology* **147**: 209–232.

Monteith, JL, **Unsworth, MH.** 2014. *Principles of environmental physics*. Oxford, UK: Academic Press: 401.

Munger, JW, **Wofsy, SC**, **Bakwin, PS**, **Fan, S-M**, **Goulden, ML**, **Daube, BC**, **Goldstein, AH**, **Moore, KE**, **Fitzjarrald, DR.** 1996. Atmospheric deposition of reactive nitrogen oxides and ozone in a temperate deciduous forest and a subarctic woodland 1. Measurements and mechanisms. *Journal of Geophysical Research* **101**(D7): 12639–12657. DOI: http://dx.doi.org/10.1029/96JD00230.

Neirynck, J, **Gielen, B**, **Janssens, IA**, **Ceulemans, R.** 2012. Insights into ozone deposition patterns from decade-long ozone flux measurements over a mixed temperate forest. *Journal of Environmental Monitoring* **14**: 1684–1695.

Neirynck, J, **Verstraeten, A.** 2018. Variability of ozone deposition velocity over a mixed suburban temperate forest. *Frontiers in Environmental Science* **6**: 82. DOI: http://dx.doi.org/10.3389/fenvs.2018.00082.

Nemitz, E, **Langford, B**, **Di Marco, CF**, **Coyle, M**, **Braban, C**, **Twigg, M**, **Gerosa, G**, **Finco, A**, **Valach, A**, **Acton, J**, **Loubet, B**, **Schallart, S**, **Gasche, S**, **Diaz-Pines, E**, **Fares, S**, **Westerlund, J**, **Hallquist, Å**, **Gritsch, C**, **Zechmeister-Boltenstern, S**, **Sutton, MA.** 2013. Quantifying chemical interactions in a forest canopy—First results from the ÉCLAIRE campaign at Bosco Fontana, Po valley. Proceeding of the 4th ACCENT Symposium, 17–20 September 2013, Urbino, Italy.

Neumann, HH, **Den Hartog, G.** 1985. Eddy correlation measurements of atmospheric fluxes of ozone, sulphur, and particulates during the champaign intercomparison study. *Journal of Geophysical Research* **90**: 2097–2110.

Peterken, GF. 1996. *Natural woodland: Ecology and conservation in northern temperate regions*. Cambridge, UK: Cambridge University Press: 522.

Potier, E, **Loubet, B**, **Durand, B**, **Flura, D**, **Bourdat-Deschamps, M**, **Ciuraru, R**, **Ogée, J.** 2017. Chemical reaction rates of ozone in water infusions of wheat, beech, oak and pine leaves of different ages. *Atmospheric Environment* **151**: 176–187. DOI: http://dx.doi.org/10.1016/j.atmosenv.2016.11.069.

Potier, E, **Ogée, J**, **Jouanguy, J**, **Lamaud, E**, **Stella, P**, **Personne, E**, **Durand, B**, **Mascher, N**, **Loubet, B.** 2015. Multilayer modelling of ozone fluxes on winter wheat reveals large deposition on wet senescing leaves. *Agricultural and Forest Meteorology* **211–212**: 58–71. DOI: http://dx.doi.org/10.1016/j.agrformet.2015.05.006.

Rannik, Ü, **Altimir, N**, **Mammarella, I**, **Bäck, J**, **Rinne, J**, **Ruuskanen, TM**, **Hari, P**, **Vesala, T**, **Kulmala, M**. 2012. Ozone deposition into a boreal forest over a decade of observations: Evaluating deposition partitioning and driving variables. *Atmospheric Chemistry and Physics* **12**(24): 12165–12182. DOI: http://dx.doi.org/10.5194/acp-12-12165-2012.

Resco de Dios, V, **Roy, J**, **Ferrio, JP**, **Alday, JG**, **Landais, D**, **Milcu, A**, **Gessler, A.** 2015. Processes driving nocturnal transpiration and implications for estimating land evapotranspiration. *Scientific Reports* **5**: 10975.

Rummel, U, **Ammann, C**, **Kirkman, GA**, **Moura, MAL**, **Foken, T**, **Andreae, MO**, **Meixner, FX.** 2007. Seasonal variation of ozone deposition to a tropical rain forest in southwest Amazonia. *Atmospheric Chemistry and Physics* **7**: 5415–5435. DOI: http://dx.doi.org/10.5194/acp-7-5415-2007.

Schallhart, S, **Rantala, P**, **Nemitz, E**, **Taipale, D**, **Tillmann, R**, **Mentel, TF**, **Loubet, B**, **Gerosa, G**, **Finco, A**, **Rinne, J**, **Ruuskanen, TM.** 2016. Characterization of total ecosystem-scale biogenic VOC exchange at a Mediterranean oak-hornbeam forest. *Atmospheric Chemistry and Physics* **16**: 7171–7194. DOI: http://dx.doi.org/10.5194/acp-16-7171-2016.

Schotanus, P, **Nieuwstadt, F**, **De Bruin, HAR.** 1983. Temperature measurement with a sonic anemometer and its application to heat and moisture fluxes. *Boundary-Layer Meteorology* **26**: 81–93.

Simpson, D, **Benedictow, A**, **Berge, H**, **Bergstroüm, R**, **Emberson, LD**, **Fagerli, H**, **Flechard, CR**, **Hayman, GD**, **Gauss, M**, **Jonson, JE**, **Jenkin, ME**, **Nýıri, A**, **Richter, C**, **Semeena, VS**, **Tsyro, S**, **Tuovinen, J-P**, **Valdebenito, Á**, **Wind, P.** 2012. The EMEP MSC-W chemical transport model–Technical description. *Atmospheric Chemistry and Physics* **12**: 7825–7865.

Stella, P, **Loubet, B**, **Lamaud, E**, **Laville, P**, **Cellier, P.** 2011. Ozone deposition onto bare soil: A new parameterisation. *Agricultural and Forest Meteorology* **151**: 669–681.

Sun, S, **Moravek, A**, **Trebs, I**, **Kesselmeier, J**, **Sörgel, M.** 2016. Investigation of the influence of liquid surface films on O_3 and PAN deposition to plant leaves coated with organic/inorganic solution. *Journal of Geophysical Research: Atmospheres* **121**: 14239–14256. DOI: http://dx.doi.org/10.1002/2016JD025519.

Vickers, D, **Mahrt, L.** 1997. Quality control and flux sampling problems for tower and aircraft data. *Journal of Atmospheric and Oceanic Technology* **14**: 512–526.

Visser, AJ, **Ganzeveld, LN**, **Goded, I**, **Krol, MC**, **Mammarella, I**, **Manca, G**, **Folkert Boersma, K**. 2021. Ozone deposition impact assessments for forest canopies require accurate ozone flux partitioning on diurnal timescales. *Atmospheric Chemistry and Physics* **21**: 18393–18411.

Walton, S, **Gallagher, MW**, **Duyzer, JH.** 1997. Use of a detailed model to study the exchange of NO_x and O_3 above and below a deciduous canopy. *Atmospheric Environment* **31**: 2915–2931.

Wang, L, **Good, SP**, **Caylor, KK**. 2014. Global synthesis of vegetation control on evapotranspiration partitioning. *Geophysical Research Letters* **41**: 6753–6757.

Webb, EK, **Pearman, GI**, **Leuning, R**. 1980. Correction of flux measurements for density effects due to heat and water vapour transfer. *Quarterly Journal of Royal Meteorology Society* **106**: 85–100.

Wei, Z, **Yoshimura, K**, **Wang, L**, **Miralles, DG**, **Jasechko, S**, **Lee, X**. 2017. Revisiting the contribution of transpiration to global terrestrial evapotranspiration. *Geophysical Research Letters* **44**: 2792–2801.

Wesely, ML, **Eastman, A**, **Cook, DR**, **Hicks, B.** 1978. Daytime variations of ozone eddy fluxes to maize. *Boundary Layer Meteorology* **15**: 361–373.

Wittig, VE, **Ainsworth, EA**, **Naidu, SL**, **Karnosky, DF**, **Long, SP.** 2009. Quantifying the impact of current and future tropospheric ozone on tree biomass, growth, physiology and biochemistry: A quantitative meta-analysis. *Global Change Biology* **15**: 396–424.

Zhang, L, **Brook, JR**, **Vet, R.** 2002. On ozone dry deposition, with emphasis on non-stomatal uptake and wet canopies. *Atmospheric Environment* **36**: 4787–4799.

Zhang, L, **Vet, R**, **Brook, JR**, **Legge, AH.** 2006. Factors affecting stomatal uptake of ozone by different canopies and a comparison between dose and exposure. *Science of the Total Environment* **370**: 117–132.

Zona, D, **Gioli, B**, **Fares, S**, **De Groote, T**, **Pilegaard, K**, **Ibrom, A**, **Ceulemans, R.** 2014. Environmental controls on ozone fluxes in a poplar plantation in Western Europe. *Environmental Pollution* **184**: 201–210.

How to cite this article: Gerosa, GA, Marzuoli, R, Finco, A. 2022. Interannual variability of ozone fluxes in a broadleaf deciduous forest in Italy. *Elementa: Science of the Anthropocene* 10(1). DOI: https://doi.org/10.1525/elementa.2021.00105

Domain Editor-in-Chief: Detlev Helmig, Boulder AIR LLC, Boulder, CO, USA

Associate Editor: Daniel Liptzin, Soil Health Institute, Morrisville, NC, USA

Knowledge Domain: Atmospheric Science

Published: September 28, 2022 **Accepted:** August 23, 2022 **Submitted:** November 9, 2021

ELEMENTA Science of the Anthropocene

Elem Sci Anth is a peer-reviewed open access journal published by University of California Press.

OPEN ACCESS